https://doi.org/10.5194/gmd-2020-32
Preprint. Discussion started: 9 March 2020

Geoscientific Model Development Discussions

Oceanic and atmospheric methane cycling in the cGENIE Earth system model

Christopher T. Reinhard[1,2,3*], Stephanie L. Olson[2,4,5], Sandra Kirtland Turner[6], Cecily Pälike[7], Yoshiki Kanzaki[6], Andy Ridgwell[6]

[1]School of Earth and Atmospheric Sciences, Georgia Institute of Technology, Atlanta, GA 30332
[2]NASA Astrobiology Institute, Alternative Earths Team, Riverside, CA
[3]NASA Nexus for Exoplanet System Science (NExSS) Upside-Down Biospheres Team, Georgia Institute of Technology, Atlanta, GA
[4]Department of Geophysical Sciences, University of Chicago, Chicago, IL 60637
[5]Department of Earth, Atmospheric, and Planetary Science, Purdue University, West Lafayette, IN 47907
[6]Department of Earth Sciences, University of California, Riverside, Riverside, CA 92521
[7]MARUM Center for Marine Environmental Sciences, University of Bremen, Germany

*To whom correspondence should be addressed. E-mail: chris.reinhard@eas.gatech.edu

Abstract: The methane (CH_4) cycle is a key component of the Earth system that links planetary climate, biological metabolism, and the global biogeochemical cycles of carbon, oxygen, sulfur, and hydrogen. However, currently lacking is a numerical model capable of simulating a diversity of environments in the ocean where CH_4 can be produced and destroyed, and with the flexibility to be able to explore not only relatively recent perturbations to Earth's CH_4 cycle but also to probe CH_4 cycling and associated climate impacts under the very low-O_2 conditions characteristic of most of Earth history and likely widespread on other Earth-like planets. Here, we present a refinement and expansion of the ocean-atmosphere CH_4 cycle in the intermediate-complexity Earth system model cGENIE, including parameterized atmospheric O_2-O_3-CH_4 photochemistry and schemes for microbial methanogenesis, aerobic methanotrophy, and anaerobic oxidation of methane (AOM). We describe the model framework, compare model parameterizations against modern observations, and illustrate the flexibility of the model through a series of example simulations. Though we make no attempt to rigorously tune default model parameters, we find that simulated atmospheric CH_4 levels and marine dissolved CH_4 distributions are generally in good agreement with empirical constraints for the modern and recent Earth. Finally, we illustrate the model's utility in understanding the time-dependent behavior of the CH_4 cycle resulting from transient carbon injection into the atmosphere, and present model ensembles that examine the effects of atmospheric pO_2, oceanic dissolved SO_4^{2-}, and the thermodynamics of microbial metabolism on steady-state atmospheric CH_4 abundance. Future model developments will address the sources and sinks of CH_4 associated with the terrestrial biosphere and marine CH_4 gas hydrates, both of which will be essential for comprehensive treatment of Earth's CH_4 cycle during geologically recent time periods.

1. Introduction

The global biogeochemical cycle of methane (CH_4) is central to the evolution and climatic stability of the Earth system. Methane provides an important substrate for microbial metabolism, particularly in energy-limited microbial ecosystems in the deep subsurface (Valentine, 2011;Chapelle et al., 1995) and in anoxic marine and lacustrine sediments (Lovley et al.,

https://doi.org/10.5194/gmd-2020-32
Preprint. Discussion started: 9 March 2020

1982;Hoehler et al., 2001). Indeed, the microbial production and consumption of CH_4 are amongst the oldest metabolisms on Earth, with an isotopic record of bacterial methane cycling stretching back nearly 3.5 billion years (Ueno et al., 2006;Hinrichs, 2002;Hayes, 1994). As the most abundant hydrocarbon in Earth's atmosphere CH_4 also has a significant influence on atmospheric photochemistry (Thompson and Cicerone, 1986), and because it absorbs in a window region of Earth's longwave emission spectrum it is an important greenhouse gas. This has important implications over the coming centuries, with atmospheric CH_4 classified as a critical near-term climate forcing (Myhre et al., 2013), but has also resulted in dramatic impacts during certain periods of Earth history. For example, high steady-state atmospheric CH_4 has been invoked as an important component of Earth's early energy budget, potentially helping to offset a dim early Sun (Sagan and Mullen, 1972;Pavlov et al., 2000;Haqq-Misra et al., 2008), while time-dependent changes to the atmospheric CH_4 inventory have been invoked as drivers of extreme climatic perturbations throughout Earth history (Dickens et al., 1997;Dickens, 2003;Bjerrum and Canfield, 2011;Zeebe, 2013;Schrag et al., 2002). Because it is cycled largely through biological processes on the modern (and ancient) Earth and is spectrally active, atmospheric CH_4 has also been suggested as a remotely detectable biosignature that could be applied to planets beyond our solar system (Hitchcock and Lovelock, 1967;Sagan et al., 1993;Krissansen-Totton et al., 2018).

A number of low-order Earth system models incorporating a basic CH_4 cycle have been developed, particularly with a view to addressing relatively 'deep time' geological questions. These include explorations of long-term changes to the chemistry of Earth's atmosphere (Claire et al., 2006;Catling et al., 2007;Bartdorff et al., 2008;Beerling et al., 2009), potential climate impacts at steady state (Kasting et al., 2001;Ozaki et al., 2018), and transient impacts of CH_4 degassing on climate (Schrag et al., 2002;Bjerrum and Canfield, 2011). In some cases these models explicitly couple surface fluxes to a model of atmospheric photochemistry (Lamarque et al., 2006;Ozaki et al., 2018;Kasting et al., 2001), but in general atmospheric chemistry is parameterized based on offline 1- or 2-D photochemical models while surface fluxes are specified arbitrarily or are based on a simple 1-box ocean-biosphere model. A range of slightly more complex 'box' model approaches have been applied to simulate transient perturbations to Earth's CH_4 cycle and attendant climate impacts on timescales ranging from ~10^5 years (Dickens et al., 1997;Dickens, 2003) to ~10^8 years (Daines and Lenton, 2016). In addition, offline and/or highly parameterized

https://doi.org/10.5194/gmd-2020-32
Preprint. Discussion started: 9 March 2020


Geoscientific Model Development Discussions

approaches toward simulating the impact of transient CH_4 degassing from gas hydrate reservoirs have been developed and applied to relatively recent periods of Earth history (Archer and Buffett, 2005;Lunt et al., 2011) or projected future changes (Archer et al., 2009;Hunter et al., 2013). However, the most sophisticated and mechanistic models of global CH_4 cycling currently available tend to focus on terrestrial (soil or wetland) sources and sinks (Ridgwell et al., 1999;Walter and Heimann, 2000;Wania et al., 2010;Konijnendijk et al., 2011;Melton et al., 2013) or focus on explicitly modeling atmospheric photochemistry (Shindell et al., 2013).

Much less work has been done to develop ocean biogeochemistry models that are both equipped to deal with the wide range of boundary conditions characteristic of Earth history and are computationally tractable when running large model ensembles and/or on long (approaching ~10^6 year) timescales, as well as being able to simulate the (3-D) redox structure of the ocean allowing for localized zones of production and oxidation (which provides more accurate estimates of emission to the atmosphere). For instance, Elliot et al. (2011) advanced modelling of marine CH_4 cycling by developing and employing a 3-D ocean circulation and climate model (CCSM-3) to simulate the impact of injecting clathrate-derived CH_4 into the Arctic ocean. However, microbial consumption of CH_4 in the ocean interior was parameterized via an empirical log-linear function that implicitly neglects anaerobic oxidation of methane (AOM) via dissolved sulfate (SO_4^{2-}), which on the modern Earth is an enormously important internal CH_4 sink within Earth's oceans (Egger et al., 2018). Their simulations did not explore atmospheric chemistry. Similarly, Daines and Lenton (2016) also innovated over traditional box modelling approaches by applying an ocean general circulation model (GCM) to examine the role of aerobic methanotrophy in modulating ocean-atmosphere fluxes of CH_4 during Archean time (prior to ~2.5 billion years ago, Ga). However, this analysis likewise did not include AOM, and the GCM results were not coupled to atmospheric chemistry. In contrast, Olson et al. (2016) included AOM in a 3-D ocean biogeochemistry model coupled to an atmospheric chemistry routine and found that AOM represents a critical internal CH_4 sink in the oceans even at relatively low dissolved SO_4^{2-} levels. Though this represented an important further step forward in understanding marine CH_4 cycling on the early Earth, Olson et al. (2016) employed a simplified parameterization of aerobic CH_4 consumption, neglected the thermodynamics of CH_4-consuming metabolisms under energy-limited conditions, and employed a parameterization of atmospheric O_2-O_3-CH_4 photochemistry

https://doi.org/10.5194/gmd-2020-32
Preprint. Discussion started: 9 March 2020


Geoscientific Model Development Discussions

that is most readily applicable to only a subset of the atmospheric pO_2 values characteristic of Earth history (Daines and Lenton, 2016;Olson et al., 2016). While all of these studies provided new modelling innovations and advances in understanding, important facets of global CH_4 cycling, particularly as relevant to the evolution of early Earth, were lacking.

Here, we present a new framework for modeling the ocean-atmosphere biogeochemical CH_4 cycle in the 'muffin' release of the cGENIE Earth system model. Our goal is to make further progress in the development of a flexible intermediate-complexity model suitable for simulating the global biogeochemical CH_4 cycle on ocean-bearing planets, with an initial focus on periods of Earth history (or other habitable ocean-bearing planets) that lack a robust terrestrial biosphere. We also aim to provide a numerical modeling foundation from which to further develop a more complete CH_4 cycle within the cGENIE framework, including, for example, dynamic CH_4 hydrate cycling and the production/consumption of CH_4 by terrestrial ecosystems.

The outline of the paper is as follows. In Section 2 we briefly describe the GENIE/cGENIE Earth system model, with a particular eye toward the features that are most relevant for the biological carbon pump and the oceanic CH_4 cycle. In Section 3 we describe the major microbial metabolisms involved in the oceanic CH_4 cycle and compare our parameterizations to data from modern marine environments. In Section 4 we describe two alternative parameterizations of atmospheric O_2-O_3-CH_4 photochemistry incorporated into the model and compare these to modern/recent observations. In Section 5 we present results from a series of idealized simulations meant to illustrate the flexibility of the model and some potential applications. The availability of the model code, plus configuration files for all experiments described in the paper, is provided in Section 7, following a brief summary in Section 6.

2. The GENIE/cGENIE Earth system model

2.1. Ocean physics and climate model – C-GOLDSTEIN

The ocean physics and climate model in cGENIE is comprised of a reduced physics (frictional geostrophic) 3-D ocean circulation model coupled to both a 2-D energy-moisture balance model (EMBM) and a dynamic-thermodynamic sea-ice model (Edwards and Marsh, 2005;Marsh et al., 2011). The ocean model transports heat, salinity, and biogeochemical tracers using a scheme of

https://doi.org/10.5194/gmd-2020-32
Preprint. Discussion started: 9 March 2020

parameterized isoneutral diffusion and eddy-induced advection (Griffies, 1998;Edwards and Marsh, 2005;Marsh et al., 2011), exchanges heat and moisture with the atmosphere, sea ice, and land, and is forced at the ocean surface by the input of zonal and meridional wind stress according to a specified wind field. The 2-D atmospheric energy-moisture-balance model (EMBM) considers the heat and moisture balance for the atmospheric boundary layer using air temperature and specific humidity as prognostic tracers. Heat and moisture are mixed horizontally throughout the atmosphere, and exchange heat and moisture with the ocean and land surfaces with precipitation occurring above a given relative humidity threshold. The sea-ice model tracks the horizontal transport of sea ice, and the exchange of heat and freshwater with the ocean and atmosphere using ice thickness, areal fraction, and concentration as prognostic variables. Full descriptions of the model and coupling procedure can be found in Edwards and Marsh (2005) and, more recently, in Marsh et al. (2011). As implemented here, the ocean model is configured as a 36 x 36 equal-area grid (uniform in longitude and uniform in the sine of latitude) with 16 logarithmically spaced depth levels and seasonal surface forcing from the EMBM.

2.2. Ocean biological pump – BIOGEM

The biogeochemical model component — 'BIOGEM' — regulates air-sea gas exchange as well as the transformation and partitioning of biogeochemical tracers within the ocean, as described in Ridgwell et al. (2007). By default, the biological pump is driven by parameterized uptake of nutrients in the surface ocean, with this flux converted stoichiometrically to biomass that is then partitioned into either dissolved or particulate organic matter for downstream transport, sinking, and remineralization. Dissolved organic matter is transported by the ocean model and decays with a specified time constant, while particulate organic matter is immediately exported out of the surface ocean and partitioned into two fractions of differing lability. In the ocean interior, particulate organic matter is remineralized instantaneously throughout the water column following an exponential decay function with a specified remineralization length scale.

In the simulations discussed below, photosynthetic nutrient uptake in surface ocean grid cells is controlled by a single limiting nutrient, dissolved phosphate (PO_4):

$$\frac{\partial \mathrm{PO}_4}{\partial t} = -\Gamma + \lambda \mathrm{DOP}\,, \tag{1}$$

https://doi.org/10.5194/gmd-2020-32
Preprint. Discussion started: 9 March 2020

Geoscientific Model Development Discussions

$$\frac{\partial \mathrm{DOP}}{\partial t} = \upsilon \Gamma - \lambda \mathrm{DOP}\,, \tag{2}$$

where DOP represents dissolved organic phosphorus, υ represents the proportion of photosynthetic production that is initially partitioned into a dissolved organic phase, λ represents a decay constant (time^{-1}) for dissolved organic matter, and Γ represents photosynthetic nutrient uptake following Doney et al. (2006):

$$\Gamma = F_I \cdot F_N \cdot F_T \cdot (1 - f_{ice}) \cdot \frac{[\mathrm{PO_4}]}{\tau_{bio}}. \tag{3}$$

Rates of photosynthesis are regulated by terms describing the impact of available light (F_I), nutrient abundance (F_N), temperature (F_T), and fractional sea ice coverage in each grid cell (f_{ice}). Rates of photosynthetic nutrient uptake are further scaled to ambient dissolved PO_4 ($[PO_4]$) according to an optimal uptake timescale (τ_{bio}).

Note that this parameterization differs from that in Ridgwell et al. (2007). Specifically, the impacts of light and nutrient availability are both described via Michaelis-Menten terms:

$$F_I = \frac{I}{I + \kappa_I}\,, \tag{4}$$

$$F_N = \frac{[\mathrm{PO_4^{3-}}]}{\kappa_P + [\mathrm{PO_4^{3-}}]}\,, \tag{5}$$

where shortwave irradiance I is averaged over the entire mixed layer, and is assumed to decay exponentially from the sea surface with a length scale of 20 m. It is assumed that nutrient uptake and photosynthetic production only occur in surface grid cells of cGENIE (e.g., the upper 80 m), which is similar to the 'compensation depth' z_c in Doney et al. (2006) of 75 m. The terms κ_I and κ_P represent half-saturation constants for light and dissolved phosphate, respectively. In addition, the effect of temperature on nutrient uptake is parameterized according to:

$$F_T = k_{T0} \cdot \exp\left[\frac{T}{k_{eT}}\right], \tag{6}$$

where k_{T0} and k_{eT} denote pre-exponential and exponential scaling constants and T represents absolute *in-situ* temperature. The scaling constants are chosen to give approximately a factor of two change in rate with a temperature change of 10ºC (e.g., a Q_{10} response of ~2.0). Lastly, the

https://doi.org/10.5194/gmd-2020-32
Preprint. Discussion started: 9 March 2020

Geoscientific Model Development Discussions

final term in Eq. (3), not present in the default parameterization of Ridgwell et al. (2007), allows for biological productivity to scale more directly with available PO_4 when dissolved PO_4 concentrations are elevated relative to those of the modern oceans.

Particulate organic matter (POM) is immediately exported out of the surface ocean without lateral advection, and is instantaneously remineralized throughout the water column according to an exponential function of depth:

$$F_z^{POM} = F_{z=z_h}^{POM} \cdot \left(\sum_i r_i^{POM} \cdot \exp\left(\frac{z_h - z}{l_i^{POM}} \right) \right), \quad (7)$$

where F_z^{POM} is the particulate organic matter flux at a given depth (and z_h is the base of the photic zone), z is depth, r_i^{POM} and l_i^{POM} refer to the relative partitioning into each organic matter lability fraction i and the e-folding depth of that fraction, respectively. The simulations presented here employ two organic matter fractions, a 'labile' fraction (94.5%) with an e-folding depth of ~590 m and an effectively inaccessible fraction (5.5%) with an e-folding depth of 10^6 m (**Table 1**).

We employ a revised scheme for organic matter remineralization in the ocean interior, following that commonly used in models of organic matter remineralization within marine and lacustrine sediments (Rabouille and Gaillard, 1991;Van Cappellen et al., 1993;Boudreau, 1996a, b). Respiratory electron acceptors (O_2, NO_3^-, and SO_4^{2-}) are consumed according to decreasing free energy yield (Froelich et al., 1979), with consumption rates (R_i) scaled to both electron acceptor abundance and the inhibitory impact of electron acceptors with higher intrinsic free energy yield:

$$R_{O_2} = \frac{[O_2]}{\kappa_{O_2} + [O_2]}, \quad (8)$$

$$R_{NO_3} = \frac{[NO_3]}{\kappa_{NO_3} + [NO_3]} \cdot \frac{\kappa_{O_2}^i}{\kappa_{O_2}^i + [O_2]}, \quad (9)$$

$$R_{SO_4} = \frac{[SO_4]}{\kappa_{SO_4} + [SO_4]} \cdot \frac{\kappa_{O_2}^i}{\kappa_{O_2}^i + [O_2]} \cdot \frac{\kappa_{NO_3}^i}{\kappa_{NO_3} + [NO_3]}, \quad (10)$$

with the exception that in the biogeochemical configuration used here we do not consider nitrate (NO_3^-). The total consumption of settling POM within each ocean layer is governed by the predetermined remineralization profiles (Equation 7). The R_i terms denote the relative fraction of

https://doi.org/10.5194/gmd-2020-32
Preprint. Discussion started: 9 March 2020

this organic matter consumption that is performed by each respiratory process. We specify a closed system with no net organic matter burial in marine sediments (see below) and hence the POM flux to the sediment surface is assumed to be completely degraded, with the same partitioning amongst electron acceptors carried out according to local bottom water chemistry. For DOM, the assumed lifetime (λ) determines the total fraction of DOM degraded (and Equations 8-10 again determine how the consumption of electron acceptors is partitioned). The κ_i terms represent half-saturation constants for each metabolism, κ_i^j terms give inhibition constants acting on less energetic downstream respiratory processes, and brackets denote concentration. Default parameter values used here are shown in **Table 1**.

3. Oceanic methane cycling

3.1. Microbial methanogenesis

Methanogenesis represents the terminal step in our remineralization scheme, and follows the overall stoichiometry:

$$2CH_2O \rightarrow CH_4 + CO_2 \ .$$

This can be taken to implicitly include fermentation of organic matter to acetate followed by acetoclastic methanogenesis:

$$2CH_2O \rightarrow CH_3COOH \ ,$$

$$CH_3COOH \rightarrow CH_4 + CO_2 \ ,$$

or the fermentation of organic matter to acetate followed by anaerobic acetate oxidation and hydrogenotrophic methanogenesis:

$$2CH_2O \rightarrow CH_3COOH \ ,$$

$$CH_3COOH + 2H_2O \rightarrow 4H_2 + 2CO_2 \ ,$$

$$4H_2 + CO_2 \rightarrow CH_4 + 2H_2O \ ,$$

both of which have the same overall net stoichiometry provided that H_2 is assumed to be quantitatively converted to CH_4 by hydrogenotrophic methanogens. We thus ignore the scenario in which some fraction of H_2 is converted directly to biomass by hydrogenotrophic methanogens acting as primary producers (Ozaki et al., 2018).

https://doi.org/10.5194/gmd-2020-32
Preprint. Discussion started: 9 March 2020

Geoscientific Model Development Discussions

Because we specify a closed system with no net organic matter burial in marine sediments, all organic matter not remineralized by more energetic respiratory metabolisms is converted into CH_4 (e.g., $R_{CH4} = 1 - R_{O2} - R_{NO3} - R_{SO4}$):

$$R_{CH_4} = \frac{\kappa^i_{O_2}}{\kappa^i_{O_2} + [O_2]} \cdot \frac{\kappa^i_{NO_3}}{\kappa_{NO_3} + [NO_3]} \cdot \frac{\kappa^i_{SO_4}}{\kappa_{SO_4} + [SO_4]}, \quad (11)$$

where κ_i and κ_i^i terms are as described above (**Table 1**). We disable nitrate (NO_3) as a tracer in the simulations presented here, such that anaerobic remineralization of organic matter is partitioned entirely between sulfate reduction and methanogenesis (**Fig. 1**). Using our default parameter values (**Table 1**), aerobic respiration dominates organic matter remineralization at $[O_2]$ values significantly above 1 μmol kg^{-1} (**Fig. 1a**) while anaerobic remineralization is dominated by methanogenesis at $[SO_4^{2-}]$ values significantly below 1 mmol kg^{-1} (**Fig. 1b**). An important outcome of the revised 'inhibition' scheme is that metabolic pathways with differing intrinsic free energy yields can coexist, which more accurately reflects field observations from a range of natural settings (Curtis, 2003;Bethke et al., 2008;Kuivila et al., 1989;Jakobsen and Postma, 1999). In particular, it allows us to roughly capture the impact of oxidant gradients within sinking marine aggregates (Bianchi et al., 2018), which can facilitate non-trivial anaerobic carbon remineralization within sinking particles even in the presence of relatively high $[O_2]$ in the ocean water column (**Fig. 1c**).

While the model tracks the carbon isotope composition of oceanic and atmospheric CH_4 ($\delta^{13}C$, reported in per mil notation relative to the Pee Dee Belemnite, PDB), the only significant isotope effect we include here is that attendant to acetoclastic methanogenesis. We specify a constant isotope fractionation between organic carbon and CH_4 during methanogenesis of -35‰ by default (**Table 2**), which will tend to produce microbial CH_4 with a $\delta^{13}C$ composition of roughly -60‰ when combined with the default isotope fractionation associated with photosynthetic carbon fixation in the surface ocean (e.g., Kirtland Turner and Ridgwell, 2016). The model does not currently include any potential isotope effects associated with aerobic/anaerobic methanotrophy, air-sea gas exchange of CH_4, or photochemical breakdown of CH_4 in the atmosphere. It does, however, include a comprehensive ^{13}C scheme associated with ocean-atmosphere cycling of CO_2 (Kirtland Turner and Ridgwell, 2016;Ridgwell, 2001).

https://doi.org/10.5194/gmd-2020-32
Preprint. Discussion started: 9 March 2020

Geoscientific Model Development Discussions

3.2. Aerobic methanotrophy

Microbial aerobic methanotrophy proceeds according to:

$$CH_4 + 2O_2 \rightarrow CO_2 + 2H_2O$$

This reaction is highly favorable energetically, with a free energy yield under standard conditions of ~850 kJ per mole of methane consumed (**Table 2**). We represent rates of aerobic methanotrophy (R_{AER}) with a mixed kinetic-thermodynamic formulation (Jin & Bethke, 2005; 2007; Regnier et al., 2011), in which CH_4 oxidation kinetics are controlled by substrate availability, thermodynamic energy yield, and temperature:

$$R_{AER} = k_{AER} \cdot F_k^{AER} \cdot F_t^{AER} \cdot F_T \ . \tag{12}$$

A rate constant for aerobic methanotrophy (y^{-1}) is defined as k_{AER}, while F_i terms denote kinetic (k) and thermodynamic (t) factors as defined below and a temperature (T) factor as given in Eq. (6) above.

The kinetic factor (F_k) for aerobic methanotrophy is controlled by substrate availability according to:

$$F_k^{AER} = [CH_4] \cdot \frac{[O_2]}{\kappa_O^{AER} + [O_2]} \ , \tag{13}$$

where brackets denote concentration and the κ term denotes a half-saturation constant with respect to O_2. We employ a hybrid parameterization in which kinetics are first-order with respect to CH_4 but also scaled by a Michaelis-Menten-type term for O_2. This formulation is based on the rationale that half-saturation constants for CH_4 are typically similar to (or greater than) the dissolved CH_4 levels attained in anoxic water column environments (Regnier et al., 2011) but is also meant to allow for rapid CH_4 consumption under 'bloom' conditions with an appropriately scaled rate constant (see below).

The effect of thermodynamic energy yield on aerobic methanotrophy is given by:

$$F_t^{AER} = 1 - \exp\left[\frac{\Delta G_{r,AER} + \Delta G_{BQ,AER}}{\chi RT}\right], \tag{14}$$

where ΔG_r denotes the Gibbs free energy of reaction under *in-situ* conditions, ΔG_{BQ} represents the minimum energy required to sustain ATP synthesis (Hoehler et al., 2001;Hoehler, 2004;Jin and

https://doi.org/10.5194/gmd-2020-32
Preprint. Discussion started: 9 March 2020


Geoscientific Model Development Discussions

287 Bethke, 2007), χ is the stoichiometric number of the reaction (e.g., the number of times the rate-
288 determining step occurs in the overall process), and R and T represent the gas constant and absolute
289 *in-situ* temperature, respectively. The available free energy is estimated according to:

$$\Delta G_{r,AER} = \Delta G^{0}_{r,AER} + RT \cdot \ln \frac{\gamma_{CO_2}[CO_2]}{\gamma_{O_2}[O_2] \cdot \gamma_{CH_4}[CH_4]}, \quad (15)$$

290 where, in addition to the terms defined above, ΔG_r^0 represents the Gibbs free energy of the reaction
291 under standard conditions, and γ_i values represent activity coefficients. Note that we assume an
292 H_2O activity of unity.
293
294 **3.3. Anaerobic oxidation of methane (AOM)**
295 The oxidation of methane can also be coupled to electron acceptors other than O_2, including nitrate
296 (NO_3^-), sulfate (SO_4^{2-}), and oxide phases of iron (Fe) and manganese (Mn) (Reeburgh,
297 1976;Martens and Berner, 1977;Hoehler et al., 1994;Hinrichs et al., 1999;Orphan et al.,
298 2001;Sivan et al., 2011;Haroon et al., 2013;Egger et al., 2015). Because it is by far the most
299 abundant of these oxidants on the modern Earth, and has likely been the most abundant throughout
300 Earth's history, we focus on anaerobic oxidation of methane (AOM) at the expense of SO_4^{2-}:

$$CH_4 + SO_4^{2-} \rightarrow HCO_3^- + HS^- + H_2O \ .$$

301 This process is currently thought to be performed most often through a syntrophic association
302 between Archaea and sulfate reducing bacteria (Boetius et al., 2000), though the mechanics
303 controlling the exchange of reducing equivalents within the syntrophy remain to be fully elucidated
304 (Milucka et al., 2012;McGlynn et al., 2015). In any case, consumption of CH_4 at the sulfate-
305 methane transition zone (SMTZ) represents an extremely large sink flux of CH_4 in modern marine
306 sediments (Regnier et al., 2011;Egger et al., 2018).
307
308 Anaerobic methanotrophy is much less energetically favorable under standard conditions, with a
309 free energy yield of ~30 kJ per mole of CH_4 (**Table 2**). As a result, the influence of
310 thermodynamics on rates of AOM is potentially much stronger than it will tend to be in the case
311 of aerobic methanotrophy. As above, rates of AOM are controlled by the combined influence of
312 substrate availability, thermodynamic drive, and temperature:

$$R_{AOM} = k_{AOM} \cdot F_k^{AOM} \cdot F_t^{AOM} \cdot F_T \quad (16)$$

https://doi.org/10.5194/gmd-2020-32
Preprint. Discussion started: 9 March 2020

Geoscientific Model Development Discussions

where k_{AOM} is a rate constant for anaerobic methane oxidation (y^{-1}), while F_i terms denote kinetic (k) and thermodynamic (t) factors as defined below and a temperature (T) factor as given in Eq. (6) above.

The kinetics of anaerobic methane oxidation are specified according to:

$$F_k^{AOM} = [CH_4] \cdot \frac{[SO_4^{2-}]}{\kappa_S^{AOM} + [SO_4^{2-}]} \quad (17)$$

where brackets denote concentration and the κ term denotes a half-saturation constant with respect to SO_4^{2-}. We employ a hybrid parameterization in which kinetics are first-order with respect to CH_4 but are also scaled by a Michaelis-Menten-type term for SO_4^{2-} for reasons discussed above.

The effect of thermodynamic energy yield on anaerobic methane oxidation is specified as follows:

$$F_t^{AOM} = 1 - \exp\left[\frac{\Delta G_{r,AOM} + \Delta G_{BQ,AOM}}{\chi RT}\right] \quad . \quad (18)$$

As above, ΔG_r denotes the Gibbs free energy of reaction under *in-situ* conditions, ΔG_{BQ} is the minimum energy required to sustain ATP synthesis (the 'biological quantum'), χ is the stoichiometric number of the reaction, and R and T represent the gas constant and absolute *in-situ* temperature, respectively. The available free energy for AOM under *in-situ* conditions is estimated according to:

$$\Delta G_{r,AOM} = \Delta G^0_{r,AOM} + RT \cdot \ln \frac{\gamma_{HCO_3^-}[HCO_3^-] \cdot \gamma_{HS^-}[HS^-]}{\gamma_{SO_4^{2-}}[SO_4^{2-}] \cdot \gamma_{CH_4}[CH_4]} \quad , \quad (19)$$

where ΔG_r^0 again represents the Gibbs free energy of the net AOM reaction given above under standard conditions, and γ_i values represent activity coefficients. Again, we assume an H_2O activity of unity.

3.4. Default parameters for aerobic and anaerobic methanotrophy

We choose default rate constants according to a dataset of compiled rates of aerobic and anaerobic methanotrophy in oxygenated and anoxic marine water column environments (see Supplementary Data), after correction to *in-situ* temperature (**Fig. 2a, b**). Our default values for both rate constants are on the low end of the observational dataset, but are very roughly tuned to yield steady-state

https://doi.org/10.5194/gmd-2020-32
Preprint. Discussion started: 9 March 2020


Geoscientific Model Development Discussions

diffusive CH_4 fluxes from the ocean that are consistent with recent observational constraints (**Fig. 2c**). It is important to note, however, that these values are not extensively tuned and could be adjusted depending on the application. For example, transient CH_4 release experiments could employ rate constants that are scaled upward to reflect transient ('bloom') elevations in microbial community CH_4 consumption as observed in field studies (Kessler et al., 2011;Crespo-Medina et al., 2014). Default values for other kinetic parameters (**Table 2**) are chosen to be broadly consistent with field measurements and pure/mixed culture experiments with aerobic methanotrophs (Bender and Conrad, 1992, 1993;Hanson and Hanson, 1996;Dunfield and Conrad, 2000;van Bodegom et al., 2001), and to remain roughly consistent with previous work for comparative purposes (e.g., Olson et al., 2016), though the parameters have not been formally tuned and we explore model sensitivity below.

Thermodynamic energy yields of each reaction under standard conditions are calculated based on the standard molal thermodynamic properties given in Regnier et al. (2011). Stoichiometric numbers are assumed identical for both metabolisms, with default values of 1.0 (Jin and Bethke, 2005;Dale et al., 2006). We assume a default biological quantum (ΔG_{BQ}) of 15 kJ mol^{-1} for both aerobic and anaerobic methanotrophy, though these can be expected to vary somewhat as a function of metabolism and environmental conditions (Schink, 1997;Hoehler, 2004;Dale et al., 2008). These can be varied independently for aerobic and anaerobic methanotrophy in the model, and we explore model sensitivity to this parameter below. Lastly, for simplicity and to minimize computational expense we assume constant activity coefficients for each species throughout all ocean grid cells (**Table 2**). For some applications it may ultimately be important to add a scheme for estimating activity coefficients according to ambient salinity and ion chemistry, for example estimating methane fluxes in planetary scenarios with very different major ion chemistry or much higher/lower salinity than those characteristic of Earth's modern oceans.

4. Atmospheric methane cycling

4.1. Air-sea gas exchange

Ocean-atmosphere fluxes of CH_4 (J_{gas}) are governed by temperature- and salinity-dependent solubility and surface wind speed above a given grid cell:

https://doi.org/10.5194/gmd-2020-32
Preprint. Discussion started: 9 March 2020


Geoscientific Model Development Discussions

$$J_{gas} = A \cdot k_{gas} \cdot \left([CH_4]_{sat} - [CH_4]_{cell} \right) \quad , \tag{20}$$

where A denotes the area available for gas-exchange (e.g., the area of ice-free surface ocean), $[CH_4]_{cell}$ denotes the ambient dissolved CH_4 concentration in a given surface ocean grid cell, $[CH_4]_{sat}$ represents the dissolved CH_4 concentration at saturation with a given atmospheric pCH_4, temperature, and salinity, and k_{gas} represents a gas transfer velocity. Solubility is based on a Bunsen solubility coefficient (β) corrected for ambient temperature (T) and salinity (S) according to:

$$\ln \beta = a_1 + a_2(100/T) + a_3 \ln(T/300) + S\left[b_1 + b_2(T/100) + b_3(T/100)^2 \right], \tag{21}$$

[Note that the Henry's law constant K_0 is related to the Bunsen solubility coefficient by $K_0 = \beta/\rho V^+$, where ρ is density and V^+ is the molar volume of the gas at STP.] Gas transfer velocity (k_{gas}) is calculated based on the surface windspeed (u) and a Schmidt number (Sc) corrected for temperature assuming a constant salinity of 35‰:

$$k_{gas} = k \cdot u^2 \cdot \left[\mathrm{Sc}/660 \right]^{-0.5}, \tag{22}$$

where k is a dimensionless gas transfer coefficient, u is surface wind speed, and Sc is the temperature-corrected Schmidt number according to:

$$\mathrm{Sc} = c_1 - c_2 T + c_3 T^2 - c_4 T^3. \tag{23}$$

All default constants and coefficients for the gas exchange scheme are given in **Table 3**. Overall, the scheme for air-sea gas exchange of CH_4 follows by default that for other gases accounted for in BIOGEM, such as O_2 and CO_2, as described in (Ridgwell et al., 2007)

4.2. Parameterized O_2-O_3-CH_4 photochemistry

Once degassed to the atmosphere, CH_4 becomes involved in a complex series of photochemical reactions initiated by hydroxyl radical (OH) attack on CH_4 (Kasting et al., 1983;Prather, 1996;Pavlov et al., 2000;Schmidt and Shindell, 2003). Following Claire et al. (2006) and Goldblatt et al. (2006), we parameterize O_2-O_3-CH_4 photochemistry according to a bimolecular 'rate law':

$$J_{CH_4} = k_{eff} \cdot M_{O_2} \cdot M_{CH_4} \ , \tag{24}$$

where M_i terms represent the atmospheric inventories of O_2 and CH_4, respectively, and k_{eff} denotes an effective rate constant ($Tmol^{-1}\ y^{-1}$) that is itself a complicated function of atmospheric O_2, CH_4, and CO_2 (Claire et al., 2006). At each timestep, the distribution of chemical species (e.g., other than temperature and humidity) in the atmosphere is homogenized (Ridgwell et al., 2007) and k_{eff}

https://doi.org/10.5194/gmd-2020-32
Preprint. Discussion started: 9 March 2020


Geoscientific Model Development Discussions

is estimated based on the resulting instantaneous mean partial pressures of O_2 and CH_4 according to a bivariate fit to a large suite of 1-D atmospheric photochemical models. These photochemical model results (Claire, *personal communication*) are derived following Claire et al. (2006). Briefly, values for k_{eff} are computed by a 1-D model of atmospheric photochemistry assuming a range of fixed surface mixing ratios of O_2 and CH_4 and a constant atmospheric CO_2 of 10^{-2} bar. We then fit a fifth-order polynomial surface to these k_{eff} values as a function of atmospheric pO_2 and pCH_4 (**Fig. 3**).

Our default parameterization of O_2-O_3-CH_4 chemistry (C06) is fit over a pO_2 range of 10^{-14} to 10^{-1} bar, a pCH_4 range of 10^{-6} to 2 x 10^{-3} bar, and a constant high background pCO_2 of 10^{-2} bar (Claire et al., 2006). We thus truncate the atmospheric lifetime of CH_4 at a lower bound of 7.6 years in our default parametrization, and provide an alternative parameterization of photochemical CH_4 destruction at roughly modern pO_2 and pCO_2 (SS03) derived from the results of Schmidt and Shindell (2003) for use in more geologically recent, high-O_2 atmospheres (Reinhard et al., 2017) (**Fig. 4a**). Although this parameterized photochemistry scheme should represent an improvement in accuracy relative to that implemented in Olson et al. (2016) (see Daines and Lenton, 2016), it is important to point out that a range of factors that might be expected to impact the photochemical destruction rates of CH_4 in the atmosphere, including atmospheric pCO_2, the atmospheric profile of H_2O, and spectral energy distribution (SED), have not yet been rigorously assessed. Ongoing model developments in ATCHEM are aimed at implementing a more flexible and inclusive photochemical parameterization that will allow for robust use across a wider range of atmospheric compositions and photochemical environments.

As a basic test of our photochemical parameterization, we impose a terrestrial (wetland) flux of CH_4 to the atmosphere (balanced by stoichiometric consumption of CO_2 and release of O_2), and allow the oceanic and atmospheric CH_4 cycle to spin up for 20 kyr. We then compare steady-state atmospheric pCH_4 as a function of terrestrial CH_4 flux to estimates for the last glacial, preindustrial, and modern periods. Our default parameterization is relatively simple and spans a very wide range in atmospheric O_2 and CH_4 inventories. Nevertheless, both the default scheme and the alternative parameterization for recent geologic history (and analogous planetary environments) with high-pO_2/low-pCO_2 atmospheres accurately reproduce atmospheric pCH_4

https://doi.org/10.5194/gmd-2020-32
Preprint. Discussion started: 9 March 2020


Geoscientific Model Development Discussions

values given estimated glacial, preindustrial, and modern terrestrial CH_4 fluxes (**Fig. 4C**), and both display the predicted saturation of CH_4 sinks at elevated atmospheric CH_4 observed in more complex photochemical models. We note, however, the alternative parameterization tends to yield slightly higher atmospheric pCH_4 at surface fluxes greater than ~50 Tmol y^{-1} (**Fig. 4C**). (In the remainder of the manuscript, we employ the default (C06) parameterization for atmospheric O_2-O_3-CH_4 chemistry and do not discuss the simple high-pO_2/low-pCO_2 alternative further.)

5. Example applications of the new capabilities in the cGENIE model

5.1. High-pO_2 ('modern') steady state

We explore a roughly modern steady state with appropriate continental geography and simulated overturning circulation (as in Cao et al., 2009) and initialize the atmosphere with pO_2, pCO_2, and pCH_4 of [v/v] 20.95%, 278 ppm, and 700 ppb, respectively, and with globally uniform oceanic concentrations of SO_4^{2-} (28 mmol kg^{-1}) and CH_4 (1 nmol kg^{-1}). We fix globally averaged solar insolation at the modern value (1368 W m^{-2}) with seasonally variable forcing as a function of latitude, and set radiative forcing for CO_2 and CH_4 equivalent to preindustrial values in order to isolate the effects of biogeochemistry on steady state tracer distributions. The model is then spun up for 20 kyr with atmospheric pO_2 and pCO_2 (and $\delta^{13}C$ of atmospheric CO_2) restored to preindustrial values at every timestep, and with an imposed wetland flux of CH_4 to the atmosphere of 20 Tmol yr^{-1} that has a $\delta^{13}C$ value of -60‰. Atmospheric pCH_4 and all oceanic tracers are allowed to evolve freely.

Surface, benthic, and ocean interior distributions of dissolved oxygen (O_2), sulfate (SO_4^{2-}), and methane (CH_4) are shown in **Fig. 5** for our roughly modern simulation. Dissolved O_2 ($[O_2]$) approaches air saturation throughout the surface ocean, with a distribution that is largely uniform zonally and with concentrations that increase with latitude as a result of increased solubility at lower temperature near the poles (**Fig. 5a**). Benthic $[O_2]$ shows patterns similar to those expected for the modern Earth, with relatively high values in the well-ventilated deep North Atlantic, low values in the deep North Pacific and Indian oceans, and a gradient between roughly air saturation near regions of deep convection in the high-latitude Atlantic and much lower values in the tropical and northern Pacific (**Fig. 5d**). Distributions of $[O_2]$ in the ocean interior are similar to those of the modern Earth (**Fig. 5g**) with oxygen minimum zones (OMZs) at intermediate depths underlying

https://doi.org/10.5194/gmd-2020-32
Preprint. Discussion started: 9 March 2020


Geoscientific Model Development Discussions

highly productive surface waters, particularly in association with coastal upwelling at low latitudes.

Concentrations of dissolved SO_4^{2-} ($[SO_4^{2-}]$) are largely invariant throughout the ocean, consistent with its expected conservative behavior in the modern ocean as one of the most abundant negative ions in seawater (**Fig. 5**). Slightly higher concentrations in both surface and benthic fields are seen in association with outflow from the Mediterranean, and are driven by evaporative concentration (**Fig. 5b**). Benthic $[SO_4^{2-}]$ distributions show some similarity to those of $[O_2]$ (**Fig. 5e**), though again the differences are very small relative to the overall prescribed initial tracer inventory of 28 mmol kg^{-1} and disappear almost entirely when salinity-normalized (not shown). In the ocean interior, $[SO_4^{2-}]$ is largely spatially invariant with a value of approximately 28 mmol kg^{-1} (**Fig. 5h**).

Dissolved CH_4 concentrations ($[CH_4]$) in the surface and shallow subsurface ocean are much more variable, but typically on the order of ~1-2 nmol kg^{-1} with slightly elevated concentrations just below the surface, both of which are consistent with observations from the modern ocean (Reeburgh, 2007;Scranton and Brewer, 1978). The benthic $[CH_4]$ distribution shows locally elevated values up to ~300-400 nmol kg^{-1} in shallow regions of the tropical and northern Pacific and the Indian oceans (**Fig. 5f**), which is also broadly consistent with observations from shallow marine environments with active benthic CH_4 cycling (Jayakumar et al., 2001). Within the ocean interior, dissolved CH_4 can accumulate in the water column in excess of ~100 nmol kg^{-1} in association with relatively low-O_2 conditions at intermediate depths, with zonally averaged values as high as ~70 nmol kg^{-1} but more typically in the range of ~20-40 nmol kg^{-1} (**Fig. 5i**). These concentrations are comparable to those observed locally in low-O_2 regions of the modern ocean (Sansone et al., 2001;Chronopoulou et al., 2017;Thamdrup et al., 2019).

Figure 6 shows the major metabolic fluxes within the ocean's microbial CH_4 cycle for our 'modern' configuration. Methanogenesis is focused in regions characterized by relatively low $[O_2]$ and is particularly vigorou s in the Eastern Tropical Pacific, the North Pacific, and the Indian Ocean (**Fig. 6a**). The highest zonally averaged rates of methanogenesis are observed in northern tropical and subtropical latitudes, and are focused at a depth of ~1 km (**Fig. 6d**). Rates of microbial CH_4 consumption are generally spatially coupled to rates of methanogenesis, both in a column-

https://doi.org/10.5194/gmd-2020-32
Preprint. Discussion started: 9 March 2020


Geoscientific Model Development Discussions

integrated sense (**Fig. 6b, c**) and in the zonal average (**Fig. 6e, f**). This is particularly true for AOM, rates of which are highest within the core of elevated methanogenesis rates observed in the northern subtropics. Zonally averaged AOM rates of ~10-15 nmol kg^{-1} d^{-1} compare well with field measurements of AOM within oceanic OMZs (Thamdrup et al., 2019). In general, the bulk of CH_4 produced via microbial methanogenesis is consumed via AOM, either near the seafloor or within the ocean interior.

5.2. Low-pO_2 ('ancient') steady state

Next, we explore a low-pO_2 steady state, similar to the Proterozoic Earth (Reinhard et al., 2017) but played out in a modern continental configuration and overturning circulation, by initializing the atmosphere with pO_2, pCO_2, and pCH_4 of [v/v] 2.1 x 10^{-4} atm (equivalent to a value 10^{-3} times the present atmospheric level, PAL), 278 ppm, and 500 ppm, respectively, and globally uniform oceanic concentrations of SO_4^{2-} (280 µmol kg^{-1}) and CH_4 (50 µmol kg^{-1}). We again fix globally averaged solar insolation at the modern value (1368 W m^{-2}) with seasonally variable forcing as a function of latitude, and set radiative forcing for CO_2 and CH_4 equivalent to the modern preindustrial state in order to isolate the effects of biogeochemistry on steady state tracer distributions. The model is then spun up for 20 kyr with atmospheric pO_2 and pCO_2 (and $\delta^{13}C$ of atmospheric CO_2) restored to the initial values specified above at every timestep, with an imposed 'geologic' flux of CH_4 to the atmosphere of 3 Tmol yr^{-1} at a $\delta^{13}C$ value of -60‰. Atmospheric pCH_4 and all oceanic tracers are allowed to evolve freely.

Surface, benthic, and ocean interior distributions of $[O_2]$, $[SO_4^{2-}]$, and $[CH_4]$, are shown in **Fig. 7** for our low-pO_2 simulation. Dissolved O_2 concentrations are now extremely heterogeneous throughout the surface ocean, ranging over an order of magnitude from less than 1 µmol kg^{-1} to over 10 µmol kg^{-1}, with concentrations that are regionally well in excess of air saturation at the prescribed pO_2 of 2.1 x 10^{-4} atm (**Fig. 7a**). Previous studies have shown that these features are not unexpected at very low atmospheric pO_2 (Olson et al., 2013; Reinhard et al., 2016). We note, however, that the distribution and maximum $[O_2]$ in our low-pO_2 simulation are both somewhat different from those presented in Olson et al. (2013) and Reinhard et al. (2016). We attribute this primarily to the different parameterizations of primary production in the surface ocean. In the biogeochemical configuration of cGENIE we adopt here, we allow rates of photosynthesis to scale

https://doi.org/10.5194/gmd-2020-32
Preprint. Discussion started: 9 March 2020


Geoscientific Model Development Discussions

more directly with available PO_4^{3-} than is the case in these previous studies (Eq. 3), which allows for higher rates of oxygen production in regions of deep mixing and relatively intense organic matter recycling below the photic zone (**Fig. 7a**). In any case, as in previous examinations of surface [O_2] dynamics at low atmospheric pO_2 (Olson et al., 2013;Reinhard et al., 2016), our regional [O_2] patterns still generally track the localized balance between photosynthetic O_2 release and consumption through respiration and reaction with inorganic reductants, rather than temperature-dependent solubility patterns (**Fig. 5a**). Within the ocean interior, O_2 is consumed within the upper few hundred meters and is completely absent in benthic settings (**Fig. 7d, g**).

In our low-pO_2 simulations we initialize the ocean with a globally uniform [SO_4^{2-}] of 280 µmol kg^{-1}, under the premise that marine SO_4^{2-} inventory should scale positively with atmospheric pO_2. With this much lower initial SO_4^{2-} inventory (i.e., 10^2 times less than the modern ocean), steady state [SO_4^{2-}] distributions are significantly more heterogeneous than in the modern, high-pO_2 case (**Fig. 7**). Ocean [SO_4^{2-}] is approximately homogeneous spatially in surface waters, even with a significantly reduced seawater inventory (**Fig. 7a**), but is strongly variable within the ocean interior (**Fig. 7e, h**). Indeed, in our low-pO_2 simulations SO_4^{2-} serves as the principal oxidant for organic matter remineralization in the ocean interior, with the result that its distribution effectively mirrors that of [O_2] in the modern case in both spatial texture and overall magnitude (compare **Fig. 7e, h** with **Fig. 5d, g**). Dissolved SO_4^{2-} in this simulation never drops to zero, a consequence of our initial 280 µmol kg^{-1} concentration of SO_4^{2-} representing the oxidative potential of 560 µmol kg^{-1} of O_2, some 3 times higher than the mean [O_2] value in the modern ocean interior (~170 µmol kg^{-1}).

Dissolved CH_4 concentrations in the surface and shallow subsurface ocean are variable but much higher than in our modern simulations, typically on the order of ~1-2 µmol kg^{-1} (**Fig. 7c**). The benthic [CH_4] distribution shows concentrations up to ~8 µmol kg^{-1}, with concentrations in excess of 1 µmol kg^{-1} pervasively distributed across the seafloor. In general, the benthic [CH_4] distribution inversely mirrors that of [SO_4^{2-}] (**Fig. 7f**), which results from the fact that in the low-pO_2 case SO_4^{2-} again serves as the principal oxidant of methane. Concentrations of CH_4 in the ocean interior can approach ~10 µmol kg^{-1}, but in the zonal average are typically less than 5 µmol kg^{-1} (**Fig. 7i**). Overall, the oceanic CH_4 inventory increases dramatically in the low-pO_2 case relative to the modern simulation, from ~4.5 Tmol CH_4 to ~1900 Tmol CH_4.

https://doi.org/10.5194/gmd-2020-32
Preprint. Discussion started: 9 March 2020


Geoscientific Model Development Discussions

Figure 8 shows the major metabolic fluxes within the ocean's microbial CH_4 cycle for our 'ancient' configuration. Column-integrated rates of microbial methanogenesis are greater than in the high-pO_2 case by up to a factor of ~10^2 (**Fig. 8a**), with methanogenesis also showing a much broader areal distribution. Within the ocean interior, rates of methanogenesis are most elevated in the upper ~1 km (**Fig. 8d**) as a consequence of elevated rates of organic carbon remineralization combined with a virtual absence of dissolved O_2 beneath the upper ~200 m. Rates of aerobic methanotrophy, which is effectively absent in the ocean interior (**Fig. 8e**), are elevated relative to those observed the high-pO_2 simulation by less than an order of magnitude and are concentrated in the tropical surface ocean near the equatorial divergence (**Fig. 8b**). In contrast, AOM is strongly coupled spatially to microbial methanogenesis, with rates that are often well over ~10^2 times higher than those observed in the high-pO_2 case (**Fig. 8c, f**). Once again, AOM dominates the consumption of CH_4 produced in the ocean interior and acts as an extremely effective throttle on CH_4 fluxes to the atmosphere. Despite a significant increase in overall oceanic CH_4 burden relative to our high-pO_2 simulation (see above and **Fig. 7i**), atmospheric pCH_4 increases only modestly from ~0.8 ppm to 6 ppm [v/v], equivalent to an additional radiative forcing of only ~2 W m^{-2}, due to efficient microbial consumption in the upper ocean.

5.3. Atmospheric carbon injection

To illustrate the capabilities of the model in exploring the time-dependent (perturbation) behavior of the CH_4 cycle, we perform a simple carbon injection experiment in which 3,000 PgC are injected directly into the atmosphere either as CH_4 or as CO_2, starting from our modern steady state. The injection is spread over 1,000 years, with an instantaneous initiation and termination of carbon input to the atmosphere. The magnitude and duration of this carbon injection, corresponding to 3 PgC y^{-1}, is meant to roughly mimic the upper end of estimates for the Paleocene-Eocene Thermal Maximum, a transient global warming event at ~56 Ma hypothesized to have been driven by emissions of CO_2 and/or CH_4 (Kirtland Turner, 2018). This flux is much lower than the current anthropogenic carbon input of ~10 PgC y^{-1} (Ciais et al., 2013). For simplicity, and because we focus on only the first 3,000 years following carbon injection, we treat the ocean-atmosphere system as closed, with the result that all injected carbon ultimately accumulates within the ocean

https://doi.org/10.5194/gmd-2020-32
Preprint. Discussion started: 9 March 2020


Geoscientific Model Development Discussions

and atmosphere rather than being removed through carbonate compensation and silicate weathering.

Following a carbon release to the atmosphere in the form of CH_4, there is an immediate and significant increase in atmospheric pCH_4 to values greater than 10 ppmv, followed by a gradual increase to a maximum of ~12 ppmv throughout the duration of the CH_4 input (**Fig. 9a**). Much of this methane is exchanged with the surface ocean and consumed by aerobic methanotrophy, while some is photochemically oxidized directly in the atmosphere, both of which lead to a significant but delayed increase in atmospheric pCO_2 (**Fig. 9b**). This increase in atmospheric pCH_4 and pCO_2 leads to an increase in global average surface air temperature (SAT) of ~7ºC (**Fig. 9d**), an increase in mean ocean temperature (MOT) of ~2ºC (**Fig. 9e**), along with significant acidification of the surface ocean (**Fig. 9c**).

The increase in atmospheric pCO_2 and drop in ocean pH are nearly identical if we instead inject the carbon as CO_2 rather than CH_4. (**Fig. 9b, c**). However, when carbon is injected as CH_4, there is an additional transient increase in global surface air temperature of ~2ºC and roughly 0.5ºC of additional whole ocean warming for the same carbon input and duration (**Fig. 9f**). This results from the fact that mole-for-mole, CH_4 is a much more powerful greenhouse gas than is CO_2, and oxidation of CH_4 to CO_2 is not instantaneous during the carbon release interval. Combined, these factors result in a disequilibrium situation in which a proportion of carbon released to the atmosphere remains in the form of CH_4 rather than CO_2, providing an enhancement of warming, especially during the duration of carbon input. This warming enhancement should be considered in past events during which CH_4 release is suspected as a key driver of warming. For instance, additional warming due to CH_4 forcing may help explain the apparent discrepancy between the amount of warming reconstructed by proxy records and proposed carbon forcing during the PETM (Zeebe et al., 2009)

5.4. Atmospheric pCH_4 on the early Earth

Using our low-pO_2 steady state as a benchmark case (**Section 5.2**), we briefly explore the sensitivity of atmospheric pCH_4 to a subset of model variables. All model ensembles are initially configured with globally homogeneous marine SO_4^{2-} and CH_4 inventories and a background

https://doi.org/10.5194/gmd-2020-32
Preprint. Discussion started: 9 March 2020


Geoscientific Model Development Discussions

geologic CH_4 flux of 3 Tmol y^{-1}, and are spun up for 20 kyr with a fixed pO_2 and pCO_2. We report atmospheric pCH_4 from the final model year. Our purpose here is not to be exhaustive or to elucidate any particular period of Earth history, but to demonstrate some of the major factors controlling the atmospheric abundance of CH_4 on a low-oxygen Earth-like planet. We present results from individual sensitivity ensembles from our benchmark low-pO_2 case over the following parameter ranges: (1) atmospheric pO_2 between 10^{-4} to 10^{-1} times the present atmospheric level (PAL), equivalent to roughly 2 x 10^{-5} and 2 x 10^{-2} atm, respectively; (2) initial marine SO_4^{2-} inventories corresponding to globally uniform seawater concentrations between 0 and 1,000 µmol kg^{-1}; and (3) biological energy quanta (BEQ) for anaerobic methane oxidation between 5 and 30 kJ mol^{-1}.

Results for our low-pO_2 sensitivity ensembles are shown in **Figure 10**. We find a similar sensitivity of atmospheric pCH_4 to atmospheric pO_2 to that observed by (Olson et al., 2016). In particular, atmospheric CH_4 abundance initially increases as atmospheric pO_2 drops below modern values to roughly 2-3% PAL, after which decreasing pO_2 causes pCH_4 to drop. This behavior is well-known from previous 1-D photochemical model analysis, and arises principally from increasing production of OH via water vapor photolysis as shielding of H_2O by ozone (O_3) decreases at low atmospheric pO_2 (Pavlov et al., 2003;Claire et al., 2006;Goldblatt et al., 2006). However, peak atmospheric pCH_4 is significantly reduced in our models relative to those of Olson et al. (2016). For example, at an 'optimal' atmospheric pO_2 of ~2.5% PAL Olson et al. (2016) predict a steady state atmospheric pCH_4 of ~35 ppmv, while we predict a value of ~10 ppmv (**Fig. 10a**). This difference can be attributed to our updated O_2-O_3-CH_4 photochemistry parameterization together with a significant upward revision in the rate constant for aerobic methanotrophy. Nevertheless, our results strongly reinforce the arguments presented in Olson et al. (2016), and taken at face value further marginalize the role of CH_4 as a significant climate regulator at steady state during most of the Proterozoic Eon (between ~2.5 and 0.5 Ga).

Atmospheric CH_4 abundance is also strongly sensitive to the marine SO_4^{2-} inventory (**Fig. 10b**). The scaling we observe between initial SO_4^{2-} inventory and steady state atmospheric pCH_4 is very similar to that reported by Olson et al. (2016), with a sharp drop in the marine CH_4 inventory and atmospheric CH_4 abundance as marine SO_4^{2-} drops below ~100 µmol kg^{-1} (**Fig. 10b**). The

https://doi.org/10.5194/gmd-2020-32
Preprint. Discussion started: 9 March 2020


Geoscientific Model Development Discussions

implication is that for most of Earth history anaerobic oxidation of CH_4 in the ocean interior has served as an important inhibitor of CH_4 fluxes from the ocean biosphere. However, during much of the Archean Eon (between 4.0 and 2.5 Ga), sulfur isotope analysis indicates that marine SO_4^{2-} concentrations may instead have been on the order of ~1-10 μmol kg^{-1} (Crowe et al., 2014), while atmospheric pO_2 would also have been much lower than the values examined here (Pavlov & Kasting, 2002). The impact of the ocean biosphere and redox chemistry on atmospheric pCH_4 and Earth's climate system may thus have been much more important prior to ~2.5 billion years ago.

Interestingly, atmospheric CH_4 is significantly impacted by the value chosen for the biological energy quantum (BEQ). With all other parameters held constant, we observe an increase in steady state atmospheric pCH_4 from ~7 ppmv to ~25 ppmv when increasing the BEQ value from 20 to 30 kJ mol^{-1} (**Fig. 10c**). This effect is mediated primarily by the importance of anaerobic methanotrophy when atmospheric pO_2 is low and the ocean interior is pervasively reducing. The standard free energy of AOM is of the same order of magnitude as the BEQ (see above), which elevates the importance of thermodynamic drive in controlling global rates of AOM. We would expect this effect to be much less important when aerobic methanotrophy is the predominant CH_4 consuming process within the ocean biosphere, as the standard free energy of this metabolism is over an order of magnitude greater than typical BEQ values for microbial metabolism (e.g., Hoehler, 2004). In any case, our results suggest that the role of thermodynamics should be borne in mind in scenarios for which AOM is an important process in the CH_4 cycle and seawater [SO_4^{2-}] is relatively low.

6. Discussion and Conclusions

The global biogeochemical cycling of CH_4 is central to the climate and redox state of planetary surface environments, and responds to the internal dynamics of other major biogeochemical cycles across a very wide range of spatial and temporal scales. There is thus strong impetus for the ongoing development of a spectrum of models designed to explore planetary CH_4 cycling, from simple box models to more computationally expensive 3-D models with dynamic and interactive ocean circulation. Our principal goal here is the development of a mechanistically realistic but simple and flexible representation of CH_4 biogeochemical cycling in Earth's ocean-atmosphere system, with the hope that this can be further developed to explore steady state and time-dependent

https://doi.org/10.5194/gmd-2020-32
Preprint. Discussion started: 9 March 2020

changes to global CH_4 cycle in Earth's past and future and ultimately to constrain CH_4 cycling dynamics on Earth-like planets beyond our solar system.

To accomplish this, we have refined the organic carbon remineralization scheme in the cGENIE Earth system model to reflect the impact of anaerobic organic matter recycling in sinking aggregates within oxygenated waters, and to include the carbon cycling and isotopic effects of microbial CH_4 production. We have also incorporated revised schemes for microbial CH_4 consumption that include both kinetic and thermodynamic constraints, and have updated the parameterized atmospheric O_2-O_3-CH_4 photochemistry to improve accuracy and for use across a wider range of atmospheric pO_2 values than that explored in previous work. Simulations of roughly modern (high-O_2) and Proterozoic (low-O_2) Earth system states demonstrate that the model effectively reproduces the first-order features of the modern ocean-atmosphere CH_4 cycle, and can be effectively implemented across a wide range of atmospheric O_2 partial pressures and marine SO_4^{2-}concentrations. In addition, our results strongly reinforce the conclusions of Olson et al. (2016) for the Proterozoic Earth system, while going beyond this to posit that the thermodynamics of anaerobic CH_4 consumption may have been important in regulating atmospheric CH_4 abundance during Archean time. Finally, our simulation of PETM-like carbon injection demonstrates the importance of explicitly considering CH_4 radiative forcing during transient warming events in Earth history.

We suggest that ongoing and future development work should focus on: (1) more rigorous tuning of organic carbon remineralization and CH_4 production/consumption schemes based on data fields from the modern ocean; (2) development and implementation of a more flexible parameterization of atmospheric photochemistry that allows the roles of atmospheric temperature structure, water vapor abundance, and atmospheric pCO_2 to be explored; (3) coupling of deep ocean chemistry with a description of marine methane hydrates and associated sedimentary CH_4 cycling; and (4) developing a representation of the production/consumption of CH_4 by terrestrial ecosystems.

https://doi.org/10.5194/gmd-2020-32
Preprint. Discussion started: 9 March 2020


Geoscientific Model Development Discussions

7. Model code availability

A manual describing code installation, basic model configuration, and an extensive series of tutorials is provided. The Latex source of the manual and PDF file can be obtained by cloning (https://github.com/derpycode/muffindoc). The user manual contains instructions for obtaining, installing, and testing the code, as well as running experiments. The version of the code used in this paper is tagged as release v0.9.10 and has a DOI of 10.5281/zenodo.3620846. Configuration files for the specific experiments presented in the paper can be found in: cgenie.muffin/genie-userconfigs/MS/reinhardetal.GMD.2020. Details of the different experiments, plus the command line needed to run each, are given in README.txt.

Author contributions:

CTR, SLO, and AR developed new model code. CTR and CP compiled and analyzed empirical data for rates of methanotrophy. CTR performed all model simulations and data analysis. CTR prepared the manuscript with contributions from all co-authors.

Acknowledgements:

CTR acknowledges support from the NASA Astrobiology Institute (NAI), the Alfred P. Sloan Foundation, and the NASA Nexus for Exoplanet System Science (NExSS). SLO acknowledges support from the T.C. Chamberlin Postdoctoral Fellowship in the Department of Geophysical Sciences at the University of Chicago. AR, SKT, and YK were supported in part by an award from the Heising-Simons Foundation. We also thank Mark Claire for providing unpublished photochemical model results.

https://doi.org/10.5194/gmd-2020-32
Preprint. Discussion started: 9 March 2020

Geoscientific Model Development Discussions

731 **TABLES:**

732

733 **Table 1.** Default parameters for organic matter production and water column remineralization.

parameter	description	default value	units	source
uptake/photosynthesis				
λ	rate constant for DOM degradation	0.5	y^{-1}	1
υ	fractional partitioning into DOM	0.66	—	1
τ_{bio}	nutrient uptake timescale	63	d	2
κ_I	light limitation term	20	W m^{-2}	3
κ_P	half-saturation constant for PO_4 uptake	2.1 x 10^{-7}	mol kg^{-1}	1
k_{T0}	pre-exponential temperature constant	0.59	—	[see text]
k_{eT}	exponential temperature constant	15.8	—	[see text]
organic remineralization				
r_1^{POM}	partitioning into labile POM fraction	0.945	—	1
l_1^{POM}	*e*-folding depth for labile POM fraction	589	m	[see text]
r_2^{POM}	partitioning into refractory POM fraction	0.055	—	4
l_2^{POM}	*e*-folding depth for recalcitrant POM fraction	10^6	m	[see text]
κ_{O_2}	half-saturation constant for aerobic respiration	1.0 x 10^{-7}	mol kg^{-1}	[see text]
$\kappa_{O_2}^i$	inhibition constant for aerobic respiration	1.0 x 10^{-6}	mol kg^{-1}	[see text]
κ_{SO_4}	half-saturation constant for sulfate reduction	5.0 x 10^{-4}	mol kg^{-1}	4
$\kappa_{SO_4}^i$	Inhibition constant for sulfate reduction	5.0 x 10^{-4}	mol kg^{-1}	4

734 [1]Ridgwell et al. (2007); [2]Meyer et al. (2016); [3]Doney et al. (2006); [4]Olson et al. (2016)

735

736

737

738

739

740

https://doi.org/10.5194/gmd-2020-32
Preprint. Discussion started: 9 March 2020

Geoscientific Model Development Discussions

741 **Table 2.** Default kinetic and thermodynamic parameters for oceanic methane cycling. Activity coefficients
742 are estimated for $T = 25$°C and $S = 35$‰.

parameter	description	default value	units	source
kinetic parameters				
k_{AER}	rate constant for aerobic methanotrophy	0.10	y^{-1}	[see text]
κ_O^{AER}	half-saturation constant for O_2	2.0×10^{-5}	mol kg^{-1}	[see text]
k_{AOM}	rate constant for AOM	0.01	y^{-1}	[see text]
κ_S^{AOM}	AOM half-saturation constant for SO_4^{2-}	5.0×10^{-4}	mol kg^{-1}	1
thermodynamic parameters				
$\Delta G^0_{r,AER}$	standard free energy yield of aerobic methanotrophy	-858.967	kJ mol^{-1}	2
$\Delta G^0_{r,AOM}$	standard free energy yield of AOM	-33.242	kJ mol^{-1}	2
$\Delta G_{BQ,AER}$	minimum free energy for aerobic methanotrophy	-15.0	kJ mol^{-1}	[see text]
$\Delta G_{BQ,AOM}$	minimum free energy for AOM	-15.0	kJ mol^{-1}	2-5
γ_{CH_4}	activity coefficient for dissolved CH_4	1.20	—	6-8
γ_{CO_2}	activity coefficient for aqueous CO_2	1.17	—	9
γ_{O_2}	activity coefficient for dissolved O_2	1.14	—	10
$\gamma_{HCO_3^-}$	activity coefficient for dissolved HCO_3^-	0.58	—	11, 12
γ_{HS^-}	activity coefficient for dissolved HS^-	0.75	—	13
$\gamma_{SO_4^{2-}}$	activity coefficient for dissolved SO_4^{2-}	0.10	—	11
R	gas constant	8.2144×10^{-3}	kJ K^{-1} mol^{-1}	
χ	stoichiometric number	1.0	—	14
isotopic parameters				
ε_{CH_4}	methanogenesis isotope effect	-35.0	‰	[see text]

743 [1]Olson et al. (2016); [2]Regnier et al. (2011); [3]Schink (1997); [4]Hoehler et al. (2001); [5]Hoehler (2004); [6]Stoessell and
744 Byrne (1982); [7]Cramer (1984); [8]Duan et al. (1992); [9]Johnson (1982); [10]Clegg and Brimblecombe (1990); [11]Ulfsbo et
745 al. (2015); [12]Berner (1965); [13]Helz et al. (2011); [14]Dale et al. (2008)

https://doi.org/10.5194/gmd-2020-32
Preprint. Discussion started: 9 March 2020

Geoscientific Model Development Discussions

746 **Table 3.** Default constants and coefficients for CH_4 gas exchange. All default parameter values derived
747 from Wanninkhof (1992). Schmidt number coefficients are for S = 35‰.

parameter	description	default value
a_1	Bunsen temperature coefficient 1	-68.8862
a_2	Bunsen temperature coefficient 2	101.4956
a_3	Bunsen temperature coefficient 3	28.7314
b_1	Bunsen salinity coefficient 1	-0.076146
b_2	Bunsen salinity coefficient 2	0.043970
b_3	Bunsen salinity coefficient 3	-0.0068672
c_1	Schmidt temperature coefficient 1	2039.2
c_2	Schmidt temperature coefficient 2	120.31
c_3	Schmidt temperature coefficient 3	3.4209
c_4	Schmidt temperature coefficient 4	0.040437
k	Gas exchange constant	0.31

748
749
750
751
752
753
754
755
756
757
758
759
760
761
762
763
764
765
766

https://doi.org/10.5194/gmd-2020-32
Preprint. Discussion started: 9 March 2020

Geoscientific Model Development Discussions
Open Access
EGU

767 **FIGURES:**

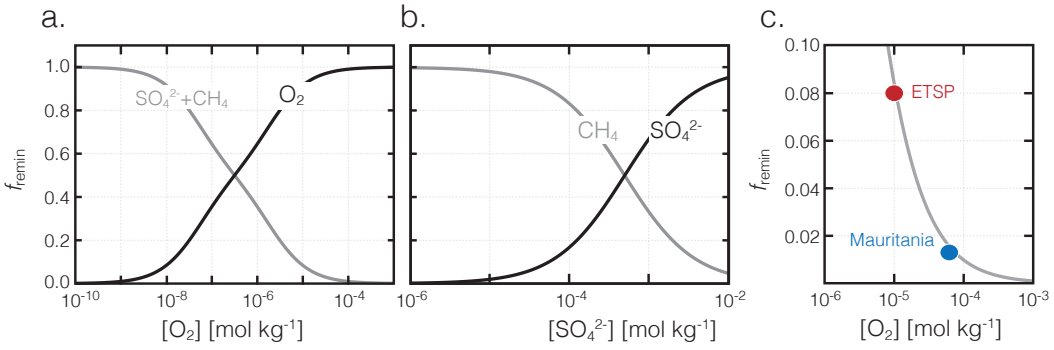

768
769
770 **Figure 1.** Fractional organic carbon remineralization by aerobic respiration, sulfate reduction, and methanogenesis in
771 our modified organic matter remineralization scheme. In (a), relative rates of aerobic (O_2) and anaerobic (SO_4^{2-} + CH_4)
772 remineralization are plotted as a function of dissolved [O_2]. In (b), relative anaerobic remineralization rates are
773 partitioned between sulfate reduction and methanogenesis as a function of dissolved [SO_4^{2-}] (dissolved [O_2] is held
774 constant at 10^{-10} mol kg^{-1}). Shown in (c) are our estimated anaerobic remineralization fractions (grey curve) compared
775 to estimates from a particle biogeochemical model applied to oxygen minimum zones (OMZs) in the Eastern Tropical
776 South Pacific (ETSP) and Mauritanian upwelling (Bianchi et al., 2018).
777
778
779
780
781
782
783
784
785
786
787
788
789
790
791
792

https://doi.org/10.5194/gmd-2020-32
Preprint. Discussion started: 9 March 2020

Geoscientific Model Development
Discussions
Open Access
EGU

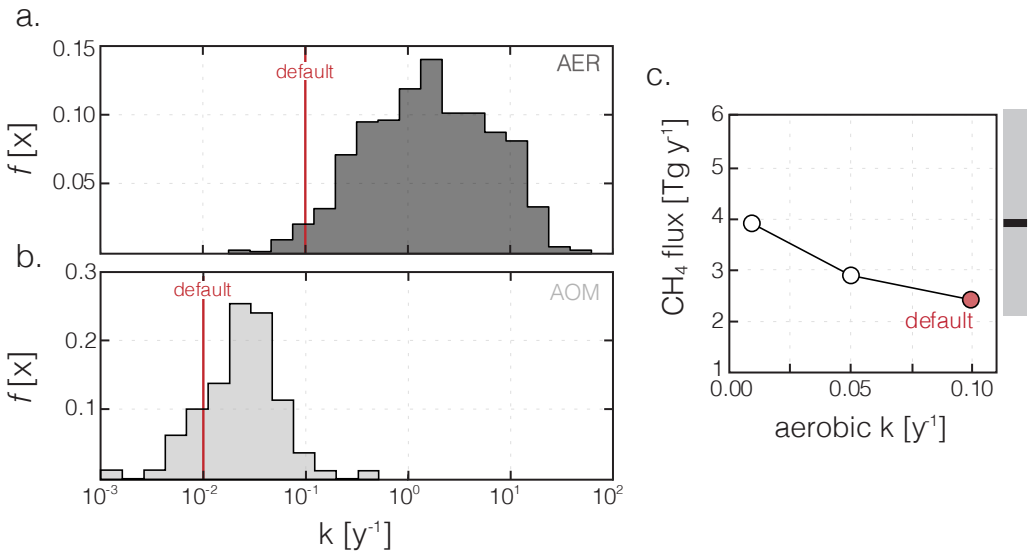

Figure 2. Compilation of rate constants for aerobic (AER; a) and anaerobic (AOM; b) methane oxidation. Rate constants are corrected for *in situ* temperature using a Q_{10} of 2 (see Supplementary Materials). Vertical red lines show our default values as reported in **Table 2**. Shown in (c) are globally integrated diffusive fluxes of CH_4 from the ocean for a range of rate constants for aerobic methanotrophy, including our default simulation. The bar to the right of (c) shows the median (black bar) and 90% credible interval (grey shading) for estimates of the modern oceanic diffusive flux from (Weber et al., 2019)

https://doi.org/10.5194/gmd-2020-32
Preprint. Discussion started: 9 March 2020

Geoscientific Model Development Discussions

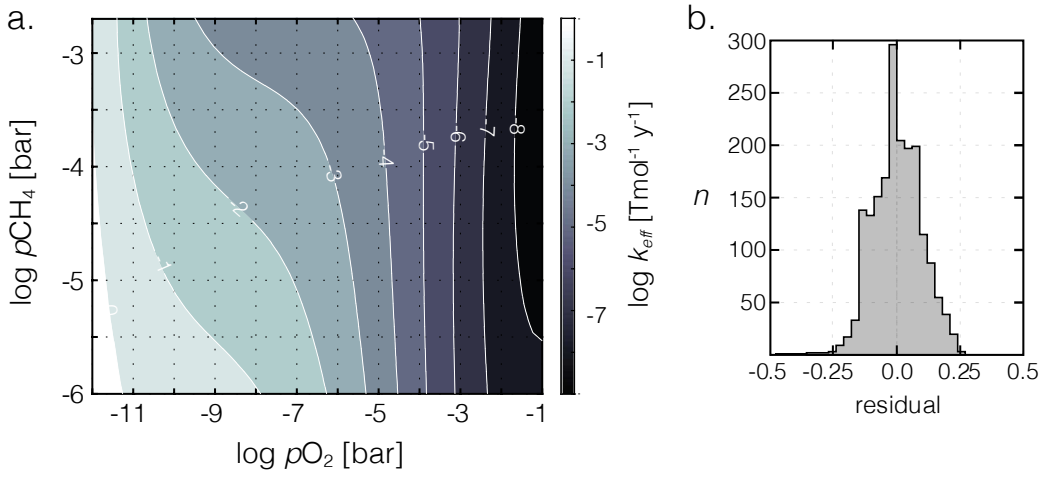

Figure 3. Shown in (a) is the bivariate fit to a suite of 1-D atmospheric photochemical runs for the effective rate constant (k_{eff}) parameterizing O_2-O_3-CH_4 photochemistry in ATCHEM. Shown in (b) is a frequency distribution of the residuals on k_{eff} from the underlying photochemical model output.

https://doi.org/10.5194/gmd-2020-32
Preprint. Discussion started: 9 March 2020

Geoscientific Model Development
Discussions
Open Access
EGU

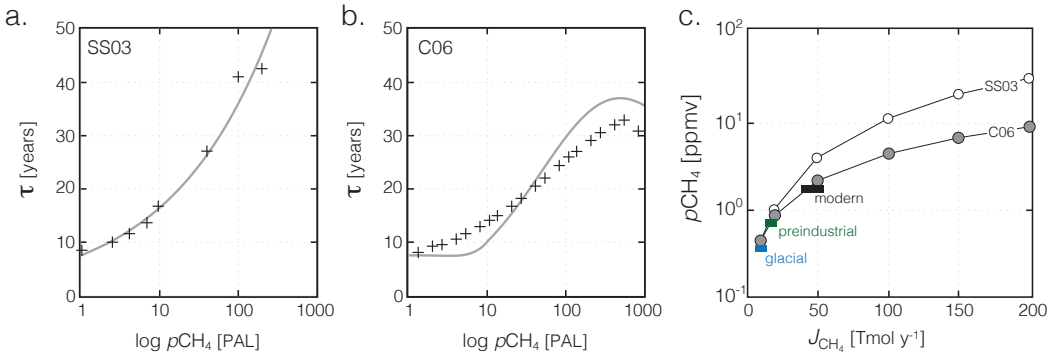

Figure 4. Comparison of steady-state atmospheric pCH_4 as a function of terrestrial CH_4 flux with modern/recent estimates. Shown in (a) is an exponential fit to the 2-D photochemistry model of Schmidt and Shindell (2003) (SS03), with individual model runs shown as black crosses. Shown in (b) is a plane through the bivariate fit shown in Figure 3 (grey curve), compared with the ensemble of 1-D atmospheric photochemical models at pO_2 = 0.1 atm (black crosses; see text). Shown in (c) are steady-state atmospheric CH_4 values as a function of imposed terrestrial CH_4 flux in our 'modern' configuration (circles), compared to estimates for the glacial, preindustrial, and modern CH_4 cycles (Kirschke et al., 2013;Bock et al., 2017;Paudel et al., 2016)

https://doi.org/10.5194/gmd-2020-32
Preprint. Discussion started: 9 March 2020

Geoscientific Model Development Discussions
Open Access
EGU

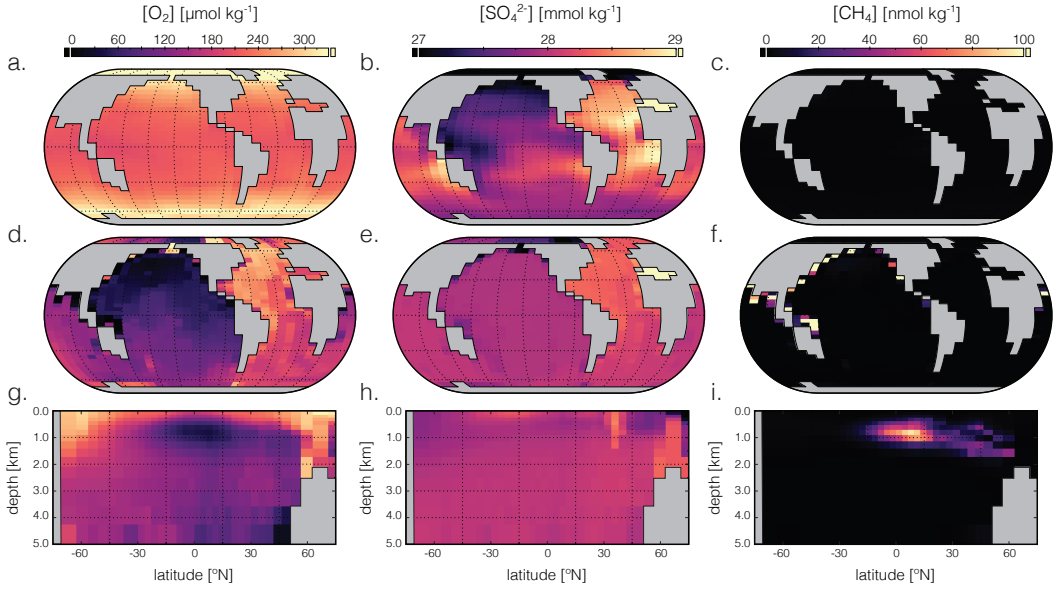

Figure 5. Tracer distributions in surface (a-c) and benthic (d-f) grid cells and in the zonally averaged ocean interior (g-i) for O_2 (a, d, g), SO_4^{2-} (b, e, h), and CH_4 (c, f, i) in our 'modern' configuration. Note different concentration units for each tracer.

https://doi.org/10.5194/gmd-2020-32
Preprint. Discussion started: 9 March 2020

Geoscientific Model Development Discussions
Open Access
EGU

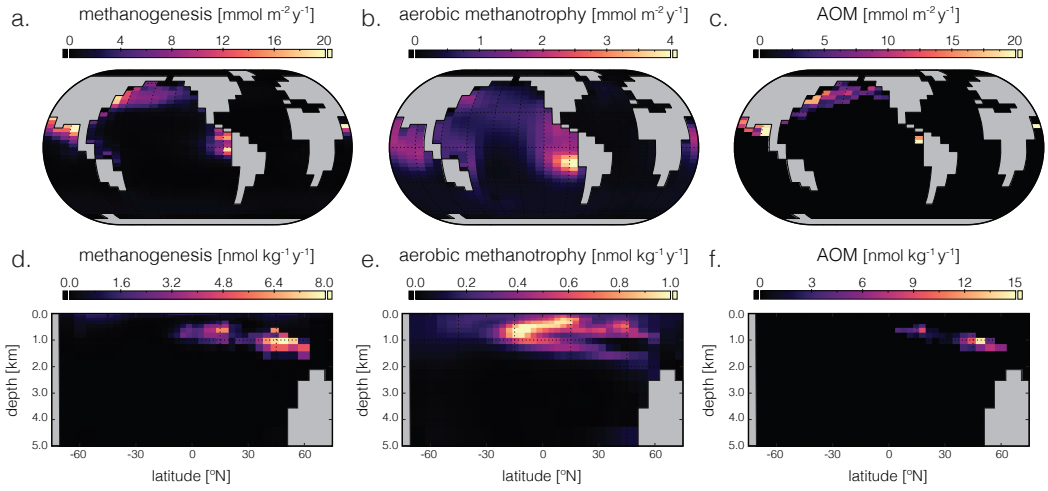

Figure 6. Major biological fluxes in the marine methane cycle for our 'modern' configuration. Panels show column integrated (a-c) and zonally averaged (d-f) rates of methanogenesis, aerobic methanotrophy, and anaerobic methane oxidation (AOM) in the ocean interior.

https://doi.org/10.5194/gmd-2020-32
Preprint. Discussion started: 9 March 2020

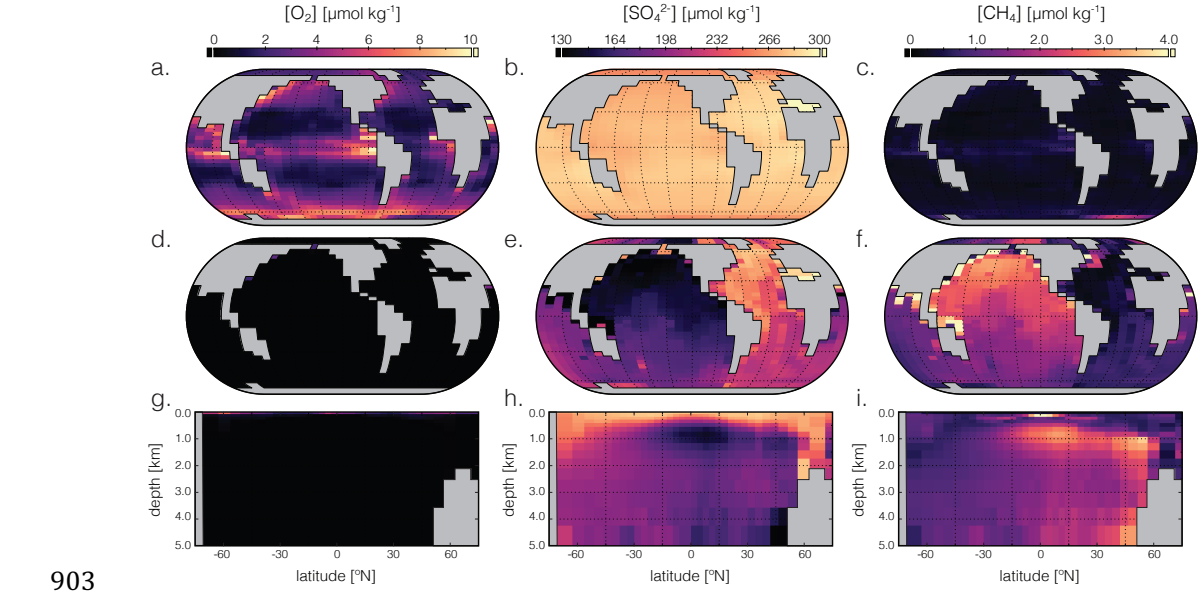

Figure 7. Tracer distributions in surface (a-c) and benthic (d-f) grid cells and in the zonally averaged ocean interior (g-i) for O_2 (a, d, g), SO_4^{2-} (b, e, h), and CH_4 (c, f, i) in our 'ancient' configuration (see text). Note different concentration units for each tracer, and the differing scales relative to Figure 5.

https://doi.org/10.5194/gmd-2020-32
Preprint. Discussion started: 9 March 2020

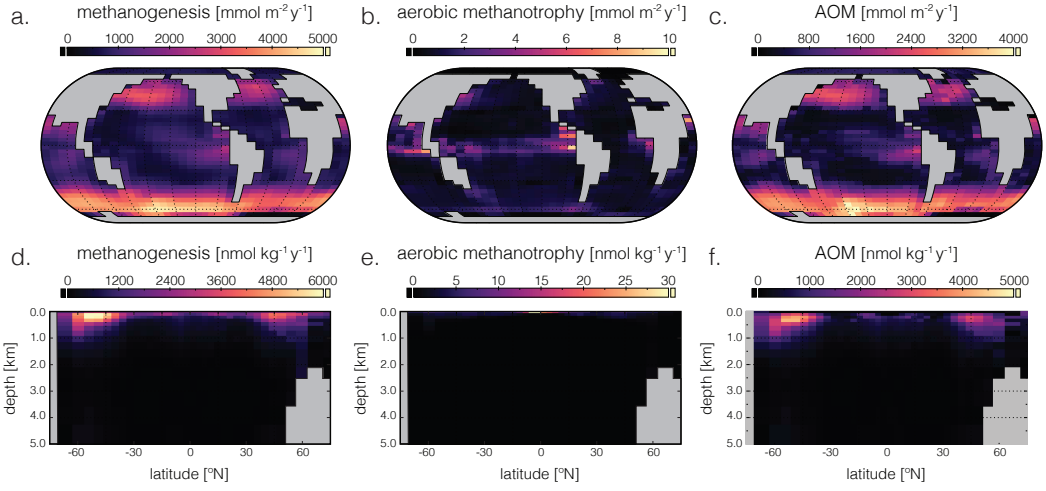

Figure 8. Major biological fluxes in the marine methane cycle for our 'ancient' configuration. Panels show column integrated (a-c) and zonally averaged (d-f) rates of methanogenesis, aerobic methanotrophy, and anaerobic methane oxidation (AOM) in the ocean interior.

https://doi.org/10.5194/gmd-2020-32
Preprint. Discussion started: 9 March 2020

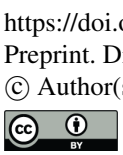

Geoscientific Model Development
Discussions
Open Access
EGU

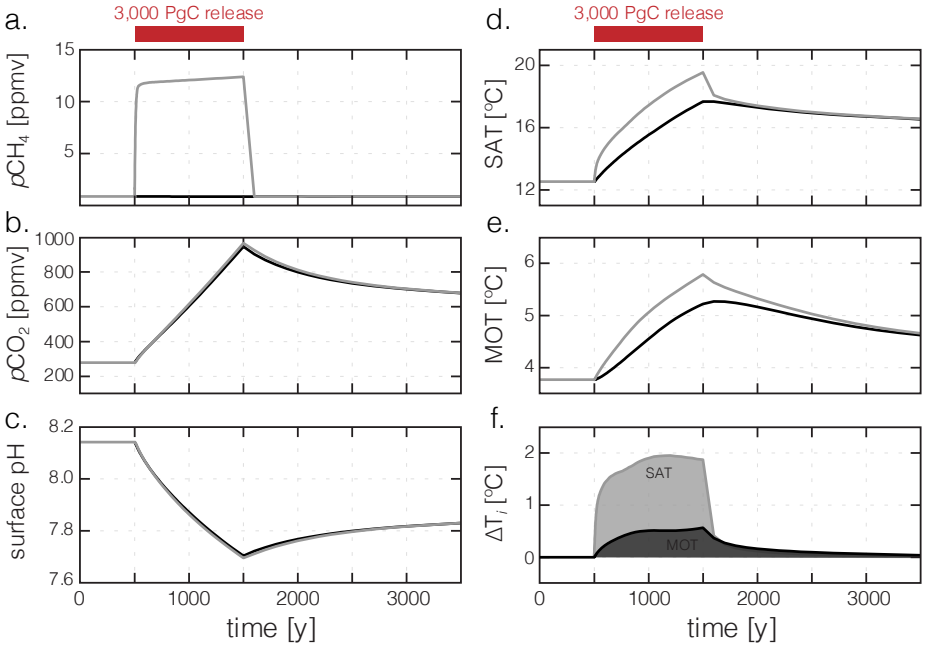

Figure 9. Response to a 3,000 PgC release directly to the atmosphere spread over 1,000 years, assuming carbon is injected as either CH_4 or CO_2. Atmospheric pCH_4 (a), pCO_2 (b), mean surface ocean pH (c), mean surface air temperature (SAT; d), and mean ocean temperature (MOT; e) are shown for a CH_4 injection (grey) and a CO_2 injection (black). Panel (f) shows the difference in SAT and MOT between the CH_4 and CO_2 injection scenarios ($\Delta T_i = T_{CH4,i} - T_{CO2,i}$) through time.

https://doi.org/10.5194/gmd-2020-32
Preprint. Discussion started: 9 March 2020

Geoscientific Model Development
Discussions
Open Access
EGU

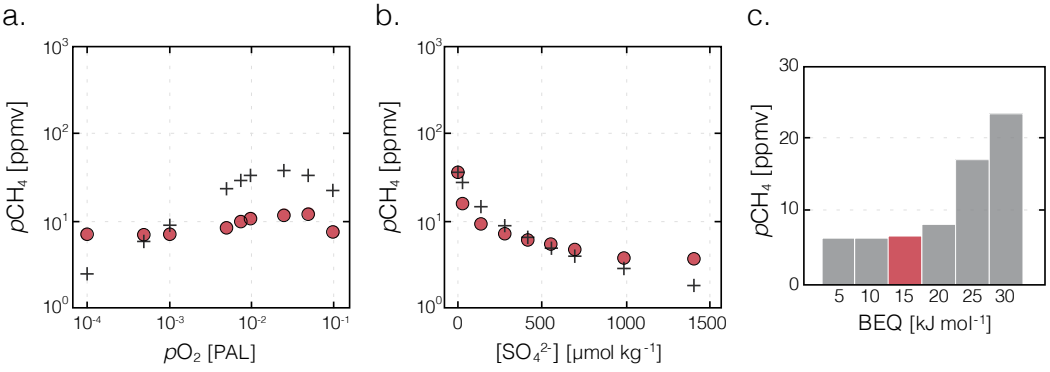

Figure 10. Sensitivity ensembles of our 'ancient' configuration compared to the results of Olson et al. (2016). Steady-state atmospheric pCH_4 values as a function of assumed atmospheric pO_2 (a) and initial marine SO_4^{2-} inventory (b) are shown for our 'ancient' configuration (filled circles; see text) and from Olson et al. (black crosses). Shown below are additional ensembles showing the impact of varying the minimum free energy yield required for microbial methane oxidation (BEQ; c) on atmospheric pCH_4. All simulations were spun up from cold for 20 kyr, with the results shown from the last model year.

https://doi.org/10.5194/gmd-2020-32
Preprint. Discussion started: 9 March 2020

Geoscientific Model Development Discussions

REFERENCES:

Archer, D., and Buffett, B.: Time-dependent response of the global ocean clathrate reservoir to climatic and anthropogenic forcing, Geochemistry Geophysics Geosystems, 6, 10.1029/2004GC000854, 2005.

Archer, D., Buffett, B., and Brovkin, V.: Ocean methane hydrates as a slow tipping point in the global carbon cycle, Proceedings of the National Academy of Sciences, USA, 106, 20596-20601, 2009.

Bartdorff, O., Wallmann, K., Latif, M., and Semenov, V.: Phanerozoic evolution of atmospheric methane, Global Biogeochemical Cycles, 22, 10.1029/2007GB002985, 2008.

Beerling, D., Berner, R. A., Mackenzie, F. T., Harfoot, M. B., and Pyle, J. A.: Methane and the CH4-related greenhouse effect over the past 400 million years, American Journal of Science, 309, 97-113, 2009.

Bender, M., and Conrad, R.: Kinetics of CH4 oxidation in oxic soils exposed to ambient air or high CH4 mixing ratios, Fems Microbiol Lett, 101, 261-270, 1992.

Bender, M., and Conrad, R.: Kinetics of methane oxidation in oxic soils, Chemosphere, 26, 687-696, 1993.

Berner, R. A.: Activity Coefficients of Bicarbonate Carbonate and Calcium Ions in Sea Water, Geochimica Et Cosmochimica Acta, 29, 947-&, 1965.

Bethke, C. M., Ding, D., Jin, Q., and Sanford, R. A.: Origin of microbiological zoning in groundwater flows, Geology, 36, 739-742, 2008.

Bianchi, D., Weber, T. S., Kiko, R., and Deutsch, C.: Global niche of marine anaerobic metabolisms expanded by particle microenvironments, Nat Geosci, 11, 263-268, 2018.

Bjerrum, C. J., and Canfield, D. E.: Towards a quantitative understanding of the late Neoproterozoic carbon cycle, Proceedings of the National Academy of Sciences, USA, 108, 5542-5547, 2011.

Bock, M., Schmitt, J., Beck, J., Seth, B., Chappellaz, J., and Fischer, H.: Glacial/interglacial wetland, biomass burning, and geologic methane emissions constrained by dual stable isotopic CH4 ice core records, Proceedings of the National Academy of Sciences, USA, 114, E5778-E5786, 2017.

Boetius, A., Ravenschlag, K., Schubert, C. J., Rickert, D., Widdel, F., Gieseke, A., Amann, R., Jørgensen, B. B., Witte, U., and Pfannkuche, O.: A marine microbial consortium apparently mediating anaerobic oxidation of methane, Nature, 407, 623-626, 2000.

Boudreau, B. P.: Diagenetic Models and Their Implementation, Springer, 1996a.

Boudreau, B. P.: A method-of-lines code for carbon and nutrient diagenesis in aquatic sediments, Computers & Geosciences, 22, 479-496, 1996b.

Cao, L., Eby, M., Ridgwell, A., Caldeira, K., Archer, D., Ishida, A., Joos, F., Matsumoto, K., Mikolajewicz, U., Mouchet, A., Orr, J. C., Plattner, G.-K., Schlitzer, R., Tokos, K., Totterdell, I., Tschumi, T., Yamanaka, Y., and Yool, A.: The role of ocean transport in the uptake of anthropogenic CO2, Biogeosciences, 6, 375-390, 2009.

Catling, D. C., Claire, M. W., and Zahnle, K. J.: Anaerobic methanotrophy and the rise of atmospheric oxygen, Philosophical Transactions of the Royal Society A, 365, 1867-1888, 2007.

Chapelle, F. H., McMahon, P. B., Dubrovsky, N. M., Fujii, R. F., Oaksford, E. T., and Vroblesky, D. A.: Deducing the distribution of terminal electron-accepting processes in hydrologically diverse groundwater systems, Water Resources Research, 31, 359-371, 1995.

https://doi.org/10.5194/gmd-2020-32
Preprint. Discussion started: 9 March 2020

1032 Chronopoulou, P.-M., Shelley, F., Pritchard, W. J., Maanoja, S., and Trimmer, M.: Origin and
1033 fate of methane in the Eastern Tropical North Pacific oxygen minimum zone, The ISME
1034 Journal, 11, 1386-1399, 2017.
1035 Ciais, P., Sabine, C., Bala, G., Bopp, L., Brovkin, V., Canadell, J., Chhabra, A., DeFries, R.,
1036 Galloway, J., Heimann, M., Jones, C., Le Quéré, C., Myneni, R. B., Piao, S., and Thornton,
1037 P.: Carbon and Other Biogeochemical Cycles, in: Climate Change 2013: The Physical
1038 Science Basis. Contribution of Working Group I to the Fifth Assessment Report of the
1039 Intergovernmental Panel on Climate Change, edited by: Stocker, T. F., Qin, D., Plattner, G.-
1040 K., Tignor, M., Allen, S. K., Boschung, J., Nauels, A., Xia, Y., Bex, V., and Midgley, P. M.,
1041 Cambridge University Press, Cambridge, 467-544, 2013.
1042 Claire, M. W., Catling, D. C., and Zahnle, K. J.: Biogeochemical modelling of the rise in
1043 atmospheric oxygen, Geobiology, 4, 239-269, 2006.
1044 Clegg, S. L., and Brimblecombe, P.: The solubility and activity coefficient of oxygen in salt
1045 solutions and brines, Geochimica et Cosmochimica Acta, 54, 3315-3328, 1990.
1046 Cramer, S. D.: Solubility of methane in brines from 0 to 300ºC, Industrial Engineering and
1047 Chemistry Process Design and Development, 23, 533-538, 1984.
1048 Crespo-Medina, M., Meile, C. D., Hunter, K. S., Diercks, A.-R., Asper, V. L., Orphan, V. J.,
1049 Tavormina, P. L., Nigro, L. M., Battles, J. J., Chanton, J. P., Shiller, A. M., Joung, D.-J.,
1050 Amon, R. M. W., Bracco, A., Montoya, J. P., Villareal, T. A., Wood, A. M., and Joye, S. B.:
1051 The rise and fall of methanotrophy following a deepwater oil-well blowout, Nat Geosci, 7,
1052 423-427, 2014.
1053 Curtis, G. P.: Comparison of approaches for simulating reactive solute transport involving
1054 organic degredation reactions by multiple terminal electron acceptors, Computers &
1055 Geosciences, 29, 319-329, 2003.
1056 Daines, S. J., and Lenton, T. M.: The effect of widespread early aerobic marine ecosystems on
1057 methane cycling and the Great Oxidation, Earth and Planetary Science Letters, 434, 42-51,
1058 2016.
1059 Dale, A. W., Regnier, P., and Van Cappellen, P.: Bioenergetic controls on anaerobic oxidation of
1060 methane (AOM) in coastal marine sediments: A theoretical analysis, American Journal of
1061 Science, 306, 246-294, 2006.
1062 Dale, A. W., Regnier, P., Knab, N. J., Jørgensen, B. B., and Van Cappellen, P.: Anaerobic
1063 oxidation of methane (AOM) in marine sediments from the Skagerrak (Denmark): II.
1064 Reaction-transport modeling, Geochimica et Cosmochimica Acta, 72, 2880-2894, 2008.
1065 Dickens, G. R., Castillo, M. M., and Walker, J. C. G.: A blast of gas in the latest Paleocene:
1066 simulating first-order effects of massive dissociation of oceanic methane hydrate, Geology,
1067 25, 259-262, 1997.
1068 Dickens, G. R.: Rethinking the global carbon cycle with a large, dynamic and microbially
1069 mediated gas hydrate capacitor, Earth and Planetary Science Letters, 213, 169-183, 2003.
1070 Doney, S. C., Lindsay, K., Fung, I., and John, J.: Natural variability in a stable, 1000-yr global
1071 coupled climate-carbon cycle simulation, Journal of Climate, 19, 3033-3054, 2006.
1072 Duan, Z., Møller, N., Greenberg, J., and Weare, J. H.: The prediction of methane solubility in
1073 natural waters to high ionic strength from 0 to 250ºC and from 0 to 1600 bar, Geochimica et
1074 Cosmochimica Acta, 56, 1451-1460, 1992.
1075 Dunfield, P. F., and Conrad, R.: Starvation alters the apparent half-saturation constant for
1076 methane in the Type II methanotroph *Methylocystis* strain LR1, Appl Environ Microb, 66,
1077 4136-4138, 2000.

https://doi.org/10.5194/gmd-2020-32
Preprint. Discussion started: 9 March 2020

1078 Edwards, N. R., and Marsh, R.: Uncertainties due to transport-parameter sensitivity in an
1079 efficient 3-D ocean-climate model, Climate Dynamics, 24, 415-433, 2005.
1080 Egger, M., Rasigraf, O., Sapart, C. J., Jilbert, T., Jetten, M. S. M., Röckmann, T., van der Veen,
1081 C., Banda, N., Kartal, B., Ettwig, K. F., and Slomp, C. P.: Iron-mediated anaerobic oxidation
1082 of methane in brackish coastal sediments, Environmental Science & Technology, 49, 277-
1083 283, 2015.
1084 Egger, M., Riedinger, N., Mogollón, J. M., and Jørgensen, B. B.: Global diffusive fluxes of
1085 methane in marine sediments, Nat Geosci, 11, 421-425, 2018.
1086 Elliot, S., Maltrud, M., Reagan, M., Moridis, G., and Cameron-Smith, P.: Marine methane cycle
1087 simulations for the period of early global warming, Journal of Geophysical Research -
1088 Biogeosciences, 116, 10.1029/2010JG001300, 2011.
1089 Froelich, P. N., Klinkhammer, G. P., Bender, M. L., Luedtke, N. A., Heath, G. R., Cullen, D.,
1090 and Duaphin, P.: Early oxidation of organic matter in pelagic sediments of the eastern
1091 equatorial Atlantic: suboxic diagenesis, Geochimica et Cosmochimica Acta, 43, 1075-1090,
1092 1979.
1093 Goldblatt, C., Lenton, T. M., and Watson, A. J.: Bistability of atmospheric oxygen and the Great
1094 Oxidation, Nature, 443, 683-686, 2006.
1095 Griffies, S. M.: The Gent-McWilliams skew flux, Journal of Physical Oceanography, 28, 831-
1096 841, 1998.
1097 Hanson, R. S., and Hanson, T. E.: Methanotrophic bacteria, Microbiological Reviews, 60, 439-
1098 471, 1996.
1099 Haqq-Misra, J., Domagal-Goldman, S. D., Kasting, P. J., and Kasting, J. F.: A revised, hazy
1100 methane greenhouse for the Archean Earth, Astrobiology, 8, 1127-1137, 2008.
1101 Haroon, M. F., Hu, S., Shi, Y., Imelfort, M., Keller, J., Hugenholtz, P., Yuan, Z., and Tyson, G.
1102 W.: Anaerobic oxidation of methane coupled to nitrate reduction in a novel archaeal lineage,
1103 Nature, 500, 567-570, 2013.
1104 Hayes, J. M.: Global methanotrophy at the Archean-Proterozoic transition, in: Proc. Nobel
1105 Symp. 84, Early Life on Earth, edited by: Bengston, S., Columbia University Press, New
1106 York, 220-236, 1994.
1107 Helz, G. R., Bura-Nakíc, E., Mikac, N., and Ciglenecki, I.: New model for molybdenum
1108 behavior in euxinic waters, Chemical Geology, 284, 323-332, 2011.
1109 Hinrichs, K.-U., Hayes, J. M., Sylva, S. P., Brewer, P. G., and DeLong, E. F.: Methane-
1110 consuming archaebacteria in marine sediments, Nature, 398, 802-805, 1999.
1111 Hinrichs, K.-U.: Microbial fixation of methane carbon at 2.7 Ga: Was an anaerobic mechanism
1112 possible?, Geochem. Geophys. Geosyst., 3, 1-10, 2002.
1113 Hitchcock, D. R., and Lovelock, J. E.: Life detection by atmospheric analysis, Icarus, 7, 149-159,
1114 1967.
1115 Hoehler, T. M., Alperin, M. J., Albert, D. B., and Martens, C. S.: Field and laboratory studies of
1116 methane oxidation in an anoxic marine sediments: Evidence for a methanogen-sulfate
1117 reducer consortium, Global Biogeochemical Cycles, 8, 451-463, 1994.
1118 Hoehler, T. M., Alperin, M. J., Albert, D. B., and Martens, C. S.: Apparent minimum free energy
1119 requirements for methanogenic Archaean and sulfate-reducing bacteria in an anoxic marine
1120 sediment, Fems Microbiol Ecol, 38, 33-41, 2001.
1121 Hoehler, T. M.: Biological energy requirements as quantitative boundary conditions for life in
1122 the subsurface, Geobiology, 2, 205-215, 2004.

https://doi.org/10.5194/gmd-2020-32
Preprint. Discussion started: 9 March 2020

1123 Hunter, S. J., Goldobin, D. S., Haywood, A. M., Ridgwell, A., and Rees, J. G.: Sensitivity of the
1124 global submarine hydrate inventory to scenarios of future climate change, Earth and
1125 Planetary Science Letters, 367, 105-115, 2013.
1126 Jakobsen, R., and Postma, D.: Redox zoning, rates of sulfate reduction and interactions with Fe-
1127 reduction and methanogenesis in a shallow sandy aquifer, Rømø, Denmark, Geochimica et
1128 Cosmochimica Acta, 63, 137-151, 1999.
1129 Jayakumar, D. A., Naqvi, S. W. A., Narvekar, P. V., and George, M. D.: Methane in coastal and
1130 offshore waters of the Arabian Sea, Marine Chemistry, 74, 1-13, 2001.
1131 Jin, Q., and Bethke, C. M.: Predicting the rate of microbial respiration in geochemical
1132 environments, Geochimica et Cosmochimica Acta, 69, 1133-1143, 2005.
1133 Jin, Q., and Bethke, C. M.: The thermodynamics and kinetics of microbial metabolism,
1134 American Journal of Science, 307, 643-677, 2007.
1135 Johnson, K. S.: Carbon dioxide hydration and dehydration kinetics in seawater, Limnology and
1136 Oceanography, 27, 849-855, 1982.
1137 Kasting, J. F., Zahnle, K. J., and Walker, J. C. G.: Photochemistry of methane in the Earth's
1138 early atmosphere, Precambrian Research, 20, 121-148, 1983.
1139 Kasting, J. F., Pavlov, A. A., and Siefert, J. L.: A coupled ecosystem-climate model for
1140 predicting the methane concentration in the Archean atmosphere, Origin of life and evolution
1141 of the Biosphere, 31, 271-285, 2001.
1142 Kessler, J. D., Valentine, D. L., Redmond, M. C., Du, M., Chan, E. W., Mendes, S. D., Quiroz,
1143 E. W., Villanueva, C. J., Shusta, S. S., Werra, L. M., Yvon-Lewis, S. A., and Weber, T. C.: A
1144 persistent oxygen anomaly reveals the fate of spilled methane in the deep Gulf of Mexico,
1145 Science, 331, 312-315, 2011.
1146 Kirschke, S., Bousquet, P., Ciais, P., Saunois, M., Canadell, J. G., Dlugokencky, E. J.,
1147 Bergamaschi, P., Bergmann, D., Blake, D. R., Bruhwiler, L., Cameron-Smith, P., Castaldi,
1148 S., Chevallier, F., Feng, L., Fraser, A., Heimann, M., Hodson, E. L., Houweling, S., Josse,
1149 B., Fraser, P. J., Krummel, P. B., Lamarque, J.-F., Langenfelds, R. L., Le Quére, C., Naik,
1150 V., O'Doherty, S., Palmer, P. I., Pison, I., Plummer, D., Poulter, B., Prinn, R. G., Rigby, M.,
1151 Ringeval, B., Santini, M., Schmidt, M., Shindell, D. T., Simpson, I. J., Spahni, R., Steele, L.
1152 P., Strode, S. A., Sudo, K., Szopa, S., van der Werf, G. R., Voulgarakis, A., van Weele, M.,
1153 Weiss, R. F., Williams, J. E., and Zeng, G.: Three decades of global methane sources and
1154 sinks, Nat Geosci, 6, 813-823, 2013.
1155 Kirtland Turner, S., and Ridgwell, A.: Development of a novel empirical framework for
1156 interpreting geological carbon isotope excursions, with implications for the rate of carbon
1157 injection across the PETM, Earth and Planetary Science Letters, 435, 1-13, 2016.
1158 Kirtland Turner, S.: Constraints on the onset duration of the Paleocene-Eocene Thermal
1159 Maximum, Philosophical Transactions of the Royal Society A, 376, 20170082, 2018.
1160 Konijnendijk, T. Y. M., Weber, S. L., Tuenter, E., and van Weele, M.: Methane variations on
1161 orbital timescales: a transient modeling experiment, Climate of the Past, 7, 635-648, 2011.
1162 Krissansen-Totton, J., Garland, R., Irwin, P., and Catling, D. C.: Detectability of biosignatures in
1163 anoxic atmospheres with the *James Webb Space Telescope*: A TRAPPIST-1e cast study, The
1164 Astrophysical Journal, 156, 114, 2018.
1165 Kuivila, K. M., Murray, J. W., and Devol, A. H.: Methane production, sulfate reduction and
1166 competition for substrates in the sediments of Lake Washington, Geochimica et
1167 Cosmochimica Acta, 53, 409-416, 1989.

https://doi.org/10.5194/gmd-2020-32
Preprint. Discussion started: 9 March 2020

1168 Lamarque, J.-F., Kiehl, J. T., Shields, C. A., Boville, B. A., and Kinnison, D. E.: Modeling the
1169 response to changes in tropospheric methane concentration: Application to the Permian-
1170 Triassic boundary, Paleoceanography, 21, 10.1029/2006PA001276, 2006.
1171 Lovley, D. R., Dwyer, D. F., and Klug, M. J.: Kinetic analysis of competition between sulfate
1172 reducers and methanogens for hydrogen in sediments, Appl Environ Microb, 43, 1373-1379,
1173 1982.
1174 Lunt, D. J., Ridgwell, A., Sluijs, A., Zachos, J. C., Hunter, S. J., and Haywood, A.: A model for
1175 orbital pacing of methane hydrate destabilization during the Palaeogene, Nat Geosci, 4, 775-
1176 778, 2011.
1177 Marsh, R., Müller, S. A., Yool, A., and Edwards, N. R.: Incorporation of the C-GOLDSTEIN
1178 efficient climate model into the GENIE framework: "eb_go_gs" configurations of GENIE,
1179 Geoscientific Model Development, 4, 957-992, 2011.
1180 Martens, C. S., and Berner, R. A.: Interstitial water chemistry of anoxic Long Island Sound
1181 sediments. 1. Dissolved gases, Limnology and Oceanography, 22, 10-25, 1977.
1182 McGlynn, S. E., Chadwick, G. L., Kempes, C. P., and Orphan, V. J.: Single cell activity reveals
1183 direct electron transfer in methanotrophic consortia, Nature, 526, 531-535, 2015.
1184 Melton, J. R., Wania, R., Hodson, E. L., Poulter, B., Ringeval, B., Spahni, R., Bohn, T., Avis, C.
1185 A., Beerling, D. J., Chen, G., Eliseev, A. V., Denisov, S. N., Hopcraft, P. O., Lettenmaier, D.
1186 P., Riley, W. J., Singarayer, J. S., Subin, Z. M., Tian, H., Zürcher, S., Brovkin, V., van
1187 Bodegom, P. M., Kleinen, T., Yu, Z. C., and Kaplan, J. O.: Present state of global wetland
1188 extent and wetland methane modelling: conclusions from a model inter-comparison project
1189 (WETCHIMP), Biogeosciences, 10, 753-788, 2013.
1190 Meyer, K. M., Ridgwell, A., and Payne, J. L.: The influence of the biological pump on ocean
1191 chemistry: implications for long-term trends in marine redox chemistry, the global carbon
1192 cycle, and marine animal ecosystems, Geobiology, 14, 207-219, 2016.
1193 Milucka, J., Ferdelman, T. G., Polerecky, L., Franzke, D., Wegener, G., Schmid, M.,
1194 Lieberwirth, I., Wagner, M., Widdel, F., and Kuypers, M. M. M.: Zero-valent sulphur is a
1195 key intermediate in marine methane oxidation, Nature, 491, 541-546, 2012.
1196 Myhre, G., Shindell, D., Breon, F.-M., Collins, W., Fuglestvedt, J., Huang, J., Koch, D.,
1197 Lamarque, J.-F., Lee, D., Mendoza, B., Nakajima, T., Robock, A., Stephens, G., Takemura,
1198 T., and Zhang, H.: Anthropogenic and natural radiative forcing, in: Climate Change 2013:
1199 The Physical Science Basis. Contribution of Working Group I to the Fifth Assessment Report
1200 of the Intergovernmental Panel on Climate Change, edited by: Stocker, T. F., Qin, D.,
1201 Plattner, G.-K., Tignor, M., Allen, S. K., Boschung, J., Nauels, A., Xia, Y., Bex, V., and
1202 Midgley, P. M., Cambridge University Press, Cambridge, 659-740, 2013.
1203 Olson, S. L., Kump, L. R., and Kasting, J. F.: Quantifying the areal extent and dissolved oxygen
1204 concentrations of Archean oxygen oases, Chemical Geology, 362, 35-43, 2013.
1205 Olson, S. L., Reinhard, C. T., and Lyons, T. W.: Limited role for methane in the mid-Proterozoic
1206 greenhouse, Proceedings of the National Academy of Sciences, USA, 113, 11447-11452,
1207 2016.
1208 Orphan, V. J., House, C. H., Hinrichs, K.-U., McKeegan, K. D., and DeLong, E. F.: Methane-
1209 consuming Archaea revealed by directly coupled isotopic and phylogenetic analysis, Science,
1210 293, 484-487, 2001.
1211 Ozaki, K., Tajika, E., Hong, P. K., Nakagawa, Y., and Reinhard, C. T.: Effects of primitive
1212 photosynthesis on Earth's early climate system, Nat Geosci, 11, 55-59, 2018.

https://doi.org/10.5194/gmd-2020-32
Preprint. Discussion started: 9 March 2020

1213 Paudel, R., Mahowald, N. M., Hess, P. G. M., Meng, L., and Riley, W. J.: Attribution of changes
1214 in global wetland methane emissions from pre-industrial to present using CLM4.5-BGC,
1215 Environmental Research Letters, 11, 034020, 10.1088/1748-9326/11/3/034020, 2016.
1216 Pavlov, A. A., Kasting, J. F., and Brown, L. L.: Greenhouse warming by CH_4 in the atmosphere
1217 of early Earth, Journal of Geophysical Research, 105, 11981-11990, 2000.
1218 Pavlov, A. A., Hurtgen, M. T., Kasting, J. F., and Arthur, M. A.: Methane-rich Proterozoic
1219 atmosphere?, Geology, 31, 87-90, 2003.
1220 Prather, M. J.: Time scales in atmospheric chemistry: Theory, GWPs for CH4 and CO, and
1221 runaway growth, Geophysical Research Letters, 23, 2597-2600, 1996.
1222 Rabouille, C., and Gaillard, J. F.: A coupled model representing the deep-sea organic carbon
1223 mineralization and oxygen consumption in surficial sediments, J Geophys Res-Oceans, 96,
1224 2761-2776, 10.1029/90jc02332, 1991.
1225 Reeburgh, W. S.: Methane consumption in Cariaco Trench waters and sediments, Earth and
1226 Planetary Science Letters, 28, 337-344, 1976.
1227 Reeburgh, W. S.: Oceanic methane biogeochemistry, Chemical Reviews, 107, 486-513, 2007.
1228 Regnier, P., Dale, A. W., Arndt, S., LaRowe, D. E., Mogollón, J., and Van Cappellen, P.:
1229 Quantitative analysis of anaerobic oxidation of methane (AOM) in marine sediments: A
1230 modeling perspective, Earth-Science Reviews, 106, 105-130, 2011.
1231 Reinhard, C. T., Planavsky, N. J., Olson, S. L., Lyons, T. W., and Erwin, D. H.: Earth's oxygen
1232 cycle and the evolution of animal life, Proceedings of the National Academy of Sciences,
1233 USA, 113, 8933-8938, 2016.
1234 Reinhard, C. T., Olson, S. L., Schwieterman, E. W., and Lyons, T. W.: False negatives for
1235 remote life detection on ocean-bearing planets: Lessons from the early Earth, Astrobiology,
1236 17, doi:10.1089/ast.2016.1598, 2017.
1237 Ridgwell, A.: Glacial-interglacial perturbations in the global carbon cycle, PhD, University of
1238 East Anglia, Norwich, UK, 2001.
1239 Ridgwell, A., Hargreaves, J. C., Edwards, N. R., Annan, J. D., Lenton, T. M., Marsh, R., Yool,
1240 A., and Watson, A.: Marine geochemical data assimilation in an efficient Earth System
1241 Model of global biogeochemical cycling, Biogeosciences, 4, 87-104, 2007.
1242 Ridgwell, A. J., Marshall, S. J., and Gregson, K.: Consumption of atmospheric methane by soils:
1243 A process-based model, Global Biogeochemical Cycles, 13, 59-70, 1999.
1244 Sagan, C., and Mullen, G.: Earth and Mars: Evolution of atmospheres and surface temperatures,
1245 Science, 177, 52-56, 1972.
1246 Sagan, C., Thompson, W. R., Carlson, R., Gurnett, D., and Hord, C.: A search for life on Earth
1247 from the Galileo spacecraft, Nature, 365, 715-721, 1993.
1248 Sansone, F. J., Popp, B. N., Gasc, A., Graham, A. W., and Rust, T. M.: Highly elevated methane
1249 in the eastern tropical North Pacific and associated isotopically enriched fluxes to the
1250 atmosphere, Geophysical Research lEtters, 28, 4567-4570, 2001.
1251 Schink, B.: Energetics of syntrophic cooperation in methanogenic degradation, Microbiology
1252 and Molecular Biology Reviews, 61, 262-280, 1997.
1253 Schmidt, G. A., and Shindell, D. T.: Atmospheric composition, radiative forcing, and climate
1254 change as a consequence of a massive methane release from gas hydrates, Paleoceanography,
1255 18, 1004, 10.1029/2002PA000757, 2003.
1256 Schrag, D. P., Berner, R. A., Hoffman, P. F., and Halverson, G. P.: On the initiation of a
1257 snowball Earth, Geochem. Geophys. Geosyst., 3, 10.1029/2001GC000219 (Available at
1258 http://www.g-cubed.org), 2002.

https://doi.org/10.5194/gmd-2020-32
Preprint. Discussion started: 9 March 2020

1259 Scranton, M. I., and Brewer, P. G.: Consumption of dissolved methane in the deep ocean,
1260 Limnology and Oceanography, 23, 1207-1213, 1978.
1261 Shindell, D. T., Pechony, O., Voulgarakis, A., Faluvegi, G., Nazarenko, L., Lamarque, J.-F.,
1262 Bowman, K., Milly, G., Kovari, B., Ruedy, R., and Schmidt, G. A.: Interactive ozone and
1263 methane chemistry in GISS-E2 historical and future climate simulations, Atmospheric
1264 Chemistry and Physics, 13, 2653-2689, 2013.
1265 Sivan, O., Adler, M., Pearson, A., Gelman, F., Bar-Or, I., John, S. G., and Eckert, W.:
1266 Geochemical evidence for iron-mediated anaerobic oxidation of methane, Limnology and
1267 Oceanography, 56, 1536-1544, 2011.
1268 Stoessell, R. K., and Byrne, P. A.: Salting-out of methane in single-salt solutions at 25ºC and
1269 below 800 psia, Geochimica et Cosmochimica Acta, 46, 1327-1332, 1982.
1270 Thamdrup, B., Steinsdóttir, H. G. R., Bertagnolli, A. D., Padilla, C. C., Patin, N. V., Garcia-
1271 Robledo, E., Bristow, L. A., and Stewart, F. J.: Anaerobic methane oxidation is an important
1272 sink for methane in the ocean's largest oxygen minimum zone, Limnology and
1273 Oceanography, 10.1002/lno.11235, 2019.
1274 Thompson, A. M., and Cicerone, R. J.: Possible perturbations to atmospheric CO, CH4, and OH,
1275 Journal of Geophysical Research, 91, 10853-10864, 1986.
1276 Ueno, Y., Yamada, K., Yoshida, N., Maruyama, S., and Isozaki, Y.: Evidence from fluid
1277 inclusions for microbial methanogenesis in the early Archaean era, Nature, 440, 516-519,
1278 2006.
1279 Ulfsbo, A., Abbas, Z., and Turner, D. R.: Activity coefficients of a simplified seawater
1280 electrolyte at varying salinity (5-40) and temperature (0 and 25ºC) using Monte Carlo
1281 simulations, Marine Chemistry, 171, 78-86, 2015.
1282 Valentine, D. L.: Emerging topics in marine methane biogeochemistry, Annual Review of
1283 Marine Science, 3, 147-171, 2011.
1284 van Bodegom, P., Stams, F., Liesbeth, M., Boeke, S., and Leffelaar, P.: Methane oxidation and
1285 the competition for oxygen in the rice rhizosphere, Appl Environ Microb, 67, 3586-3597,
1286 2001.
1287 Van Cappellen, P., Gaillard, J.-F., and Rabouille, C.: Biogeochemical transformations in
1288 sediments: Kinetic models of early diagenesis, in: Interactions of C, N, P and S
1289 Biogeochemical Cycles and Global Change, Springer, 401-445, 1993.
1290 Walter, B. P., and Heimann, M.: A process-based, climate-sensitive model to derive methane
1291 emissions from natural wetlands: Application to five wetland sites, sensitivity to model
1292 parameters, and climate, Global Biogeochemical Cycles, 14, 745-765, 2000.
1293 Wania, R., Ross, I., and Prentice, I. C.: Implementation and evaluation of a new methane model
1294 within a dynamic global vegetation model: LPJ_WHyMe v1.3.1, Geoscientific Model
1295 Development, 3, 565-584, 2010.
1296 Weber, T., Wiseman, N. A., and Kock, A.: Global ocean methane emissions dominated by
1297 shallow coastal waters, Nature Communications, 10, 4584, 10.1038/s41467-019-12541-7,
1298 2019.
1299 Zeebe, R. E., Zachos, J. C., and Dickens, G. R.: Carbon dioxide forcing alone insufficient to
1300 explain Palaeocene-Eocene Thermal Maximum warming, Nat Geosci, 2, 576-580, 2009.
1301 Zeebe, R. E.: What caused the long duration of the Paleocene-Eocene Thermal Maximum?,
1302 Paleoceanography, 28, 1-13, 10.1002/palo.20039, 2013.
1303